# FINAL REPORT

**Title:** Development of a Self-Calibrating Dissolved Oxygen Microsensor Array for the Monitoring and Control of Plant Growth in a Space Environment


**Investigators:**

Principal Investigator

Chang-Soo Kim, PhD (Assistant Professor of Electrical & Computer Engineering and Biological Sciences, University of Missouri-Rolla, Rolla, MO 65409), 573-341-4529 (voice), 573-341-4532 (fax), ckim@umr.edu

Co-Investigators

Christopher S. Brown, PhD (Director of Space Programs, Kenan Institute for Engineering, Technology & Science, North Carolina State University, Raleigh, NC)

H. Troy Nagle, PhD, MD, PE (Professor of Electrical & Computer Engineering, North Carolina State University, Raleigh, NC, Chair of Joint Department of Biomedical Engineering, North Carolina State University, Raleigh, NC, and University of North Carolina at Chapel Hill, NC)

Collaborator

D. Marshall Porterfield, PhD (Assistant Professor of Biological Sciences and Electrical & Computer Engineering, University of Missouri-Rolla, Rolla, MO)



**Period:** July 1, 2002 – January 15, 2004

**Recipient Institution:** Kenan Institute for Engineering, Technology & Science, Box 7006, North Carolina State University, Raleigh, NC 27695-7006

**Grant Number:** NAG 9-1423 (NRA-01-OBPR-01, Pilot Study, Advanced Environmental Monitoring and Control, Office of Biological and Physical Research)

## Abstract

Plant experiments in space will require active nutrient delivery concepts in which water and nutrients are replenished on a continuous basis for long-term growth. The goal of this study is to develop a novel microsensor array to provide information on the dissolved oxygen environment in the plant root zone for the optimum control of plant cultivation systems in the space environment. Control of water and oxygen is limited by the current state-of-the-art in sensor technology.

Two capabilities of the new microsensor array were tested. First, a novel *in situ* self-diagnosis/self-calibration capability for the microsensor was explored by dynamically controlling the oxygen microenvironment in close proximity to an amperometric dissolved oxygen microsensors. A pair of integrated electrochemical actuator electrodes provided the microenvironments based on water electrolysis. Miniaturized thin film dissolved oxygen microsensors on a flexible polyimide (Kapton®) substrate were fabricated and their performances were tested. Secondly, measurements of dissolved oxygen in two representative plant growth systems were made, which had not been performed previously due to lack of proper sensing technology. The responses of the oxygen microsensor array on a flexible polymer substrate properly reflected the oxygen contents on the surface of a porous tube nutrient delivery system and within a particulate substrate system. Additionally, we demonstrated the feasibility of using a 4-point thin film microprobe for water contents measurements for both plant growth systems.

The unique features of the sensor include small size and volume, multiple-point sensing, mechanical flexibility, and self-diagnosis. The proposed technology is anticipated to provide a reliable sensor feedback plant growth nutrient delivery systems in both terrestrial environment and the microgravity environment during long term space missions.

## Statement of Progress

The progress during the project period is summarized below.

(1) *In situ* self-diagnosis/self calibration capability of dissolved oxygen microsensor (see Appendices 1 and 2 for more details)

An *in situ* self-diagnosis/self-calibration technique for a dissolved oxygen microsensor was proposed in an effort to devise an intelligent microsensor system with an integrated electrochemical actuation electrode. With a built-in platinum microelectrode that surrounds the microsensor, two kinds of microenvironments, called the oxygen-saturated or the oxygen-depleted phases, can be created by water electrolysis, depending on the polarity. The functionality of the microsensor can be checked during these microenvironment phases. An amperometric dissolved oxygen microsensor was fabricated on a flexible polyimide substrate (Kapton®). The sensor responded properly to demonstrate the self-diagnosis capability during the oxygen-generating and oxygen-depleting phases. The self-calibration feature, however, suffered from two phenomena; the supersaturation of electrochemically generated dissolved gas and the influence of pH change within the microenvironment. The necessity of using the microfludic structures and the double-layered oxygen permeable membrane has been recognized to overcome these problems.

(2) Dissolved oxygen and water content measurements in a porous tube plant nutrient delivery system (see Appendices 3 and 4 for more details)

We demonstrated the feasibility of using dissolved oxygen microsensor arrays (thin film 3-electrode electrochemical cell) for oxygen detection on the surface of a porous tube nutrient delivery system. The microsensor reported the oxygen concentrations in the surface water film properly to reflect those of the solution inside the porous tube when operated at positive pressures. At negative pressures the microsensor showed convergence to zero oxygen values due to inadequate water film formation on the porous tube surface. The responses of the microsensor on the tube surface were comparable with those of a commercial miniature oxygen probe. The plan to incorporate the *in situ* self-diagnosis/self-calibration features in the plant growth monitoring system has been limited by the aforementioned reasons.

Additionally, impedance measurements were made by using a 4-point impedance microprobe (thin film 4-electrode electrochemical cell) on the same flexible substrate to determine the contents of water film on the porous tube surface. The 4-point microprobe is useful as a wetness detector as it provides a clear differentiation between dry and wet surfaces.

The experiments we conducted with the porous tube leave us a further question of the usability of these sensors in a particulate substrate nutrient delivery system. A preliminary measurement within the particulate substrate (1-2 mm Turface®) revealed that the different saturation effects are taking place due to the interactions between the substrate, air and nutrient solution, and that the microsensor undergoes saturation to a larger extent and exhibit higher sensitiveness than the commercial oxygen probe. A further study is being planned for the application of microsensors to particulate plant growth system.

## Earth Benefits

The proposed dissolved oxygen microsensor capability is expected to accomplish the functional integration (built-in on-chip intelligence) and the structural integration (miniaturization) of minimally attended biochemical monitoring system for continuous operation. This concept of an integrated sensor/actuator system will minimize maintenance requirements, as well as reduce volume, mass, and power consumption by eliminating bulky calibration systems including calibrant (fluid and gas) reservoir and flow system hardware.

Control of oxygen and water in the root zone is vital to support plant growth. The ability to control these sometimes opposing parameters in the root zone is dependent upon the availability of sensors to detect these parameters and provide feedback for control system. The unique features of the microsensor (small size, multiple-point sensing, mechanical flexibility and self-diagnosis capability) can have benefits for the study and optimization of plant cultivation systems in both terrestrial and microgravity environments.

## Bibliography

Peer-reviewed Articles

1. Chang-Soo Kim, Chae-Hyang Lee, Jason O. Fiering, Stefan Ufer, Charles W. Scarantino, H. Troy Nagle, Manipulation of microenvironment with a built-in electrochemical actuator in proximity of a dissolved oxygen microsensor, IEEE Sensors Journal, in press, 2004 (Appendix 1).
2. Sandeep Sathyan, D. Marshall Porterfield, H. Troy Nagle, Christopher S. Brown, Chang-Soo Kim, Flexible microsensor array for the root zone monitoring of porous tube plant growth system, submitted to Habitation Journal, 2004 (Appendix 2).

Peer-reviewed Abstracts

1. Chang-Soo Kim, Chae-Hyang Lee, Electrochemical and hydrodynamic interferences on the performances of an oxygen microsensor with built-in electrochemical microactuator (paper ID #42.3), IEEE Sensors 2003, p. 456-457, Toronto, Canada, Oct 22-24, 2003 (Appendix 3).
2. Chang-Soo Kim, D. Marshall Porterfield, H. Troy Nagle, Christopher S. Brown, Flexible microsensor array for the monitoring and control of plant growth environment (paper ID # MC25), Habitation 9 (3/4), p. 186, 2003, Habitation 2004, Orlando, FL, Jan 4-7, 2004 (Appendix 4).

Presentations

1. Chang-Soo Kim, Sandeep Sathyan, D. Marshall Porterfield, H. Troy Nagle, Microsensors on a flexible plastic substrate for dissolved oxygen monitoring with self-calibration capability, Abstract 330-20P (late contribution), Pittsburgh Conference on Analytical Chemistry and Applied Spectroscopy (PITTCON), Mar 9-14, 2003, Orlando, FL.
2. Chang-Soo Kim, Toward *in situ* self-diagnosis/self-calibration feature of a dissolved oxygen microsensor with an integrated electrochemical actuator, NASA AEMC Teleconference, Sep 12, 2003.

## Appendix 1 (article in press for IEEE Sensors Journal)

# Manipulation of Microenvironment with a Built-in Electrochemical Actuator in Proximity of a Dissolved Oxygen Microsensor

**Chang-Soo Kim*, Chae-Hyang Lee, Jason O. Fiering, Stefan Ufer, Charles W. Scarantino, and H. Troy Nagle**

Chang-Soo Kim, Chae-Hyang Lee: Department of Electrical and Computer Engineering and Biological sciences, University of Missouri-Rolla, Rolla, MO 65409, USA. 573-341-4529 (voice), 573-341-4532 (fax), ckim@umr.edu, leecha@umr.edu

Jason O. Fiering: Draper Laboratory, 555 Technology Square, MS 37, Cambridge MA 02139, USA. 617-258-1596, jfiering@draper.com

Stefan Ufer, H. Troy Nagle: Biomedical MicroSensors Laboratory, Department of Electrical and Computer Engineering, North Carolina State University, Raleigh, NC 27695-7911, USA., 919-515-3578 (voice), 919-513-3814 (fax), t.nagle@ncsu.edu; stufer@eos.ncsu.edu

Charles W. Scarantino: Sicel Technologies, Inc., 3800 Gateway Center Blvd. Suite 308, Morrisville, NC 27560, USA. 919-465-2236 (voice), 919-465-0153 (fax), cw.scarantino@rexhealth.com

* Corresponding author

**Abstract – Biochemical sensors for continuous monitoring require dependable periodic self-diagnosis with acceptable simplicity to check its functionality during operation. An *in situ* self-diagnostic technique for a dissolved oxygen microsensor is proposed in an effort to devise an intelligent microsensor system with an integrated electrochemical actuation electrode. With a built-in platinum microelectrode that surrounds the microsensor, two kinds of microenvironments, called the oxygen-saturated or oxygen-depleted phases, can be created by water electrolysis depending on the polarity. The functionality of the microsensor can be checked during these microenvironment phases. The polarographic oxygen microsensor is fabricated on a flexible polyimide substrate (Kapton®) and the feasibility of the proposed concept is demonstrated in a physiological solution. The sensor responds properly during the oxygen-generating and oxygen-depleting phases. The use of these microenvironments for *in situ* self-calibration is discussed to achieve functional integration as well as structural integration of the microsensor system.**

**Keywords – self-diagnosis, self-calibration, electrolysis, polyimide, intelligent microsensor.**

# I. INTRODUCTION

An intelligent microsensor system requires not only structural integration but also functional integration. In a biochemical microsensor system, special functionalities can be provided by the use of electrochemical "actuators" integrated with the sensor. Several electrochemical microactuators utilizing redox reactions of chemical species have been reported in combination with microsensors. A microscale pH titration system was first implemented by integrating a titration microelectrode with pH-ISFET (ion-sensitive field-effect transistor) [1]. Based on this concept, a long-term measurement of dissolved carbon dioxide was performed without the need for regular recalibration [2]. A similar structure has been used to demonstrate a potentiometric dissolved oxygen sensor based on pH sensing [3], which was later adopted in simultaneous measurement of cellular respiration and acidification with a single sensor [4]. With built-in iridium oxide actuators on top of the gate region of FET (field-effect transistor), novel potentiometric determinations of dissolved oxygen [5] and hydrogen peroxide [6] were accomplished. Microfludic systems including electrochemical actuators and sensors were reported to detect flow direction and to estimate flow velocity [7, 8]. Novel biosensors with built-in electrochemical actuation systems include a pH-static enzyme sensor to suppress the dependency of sensor response on sample solution pH [9] and a high-sensitivity potentiometric glucose sensor with the aid of an amperometric actuation system [10].

An ideal biosensor for long-term continuous monitoring should meet the following requirements: simple structure, immunity to motion artifacts, sufficient sensitivity for reliable measurements, robustness and stability over long periods of time, minimum inflammatory reaction with surrounding tissues during chronic implantation, and dependable diagnosis and/or calibration methods to check its functionality and accuracy. Numerous types of sensors for dissolved oxygen monitoring have been developed over the past decades (for a review, see references [11, 12]), and only limited successes have been achieved in spite of intensive efforts to meet these requirements. Apart from such long-term stability or biocompatibility, it should be emphasized that development of a novel *in situ* diagnosis technique without any externally coupled apparatus is one obstacle to the realization of an unattended intelligent microsensor system.

Consequently, we present a novel self-diagnosis concept for a dissolved oxygen microsensor by using an integrated electrochemical microactuator toward built-in intelligence of the microsensor system.

## II. *IN SITU* SELF-DIAGNOSIS CONCEPT WITH ELECTROCHEMCIAL MICROACTUATOR

The principle of the novel diagnosis method proposed herein is based on water electrolysis at noble metal electrodes as shown in Figure 1. Oxygen or hydrogen can be generated by the electrolysis of water in a controlled manner by applying voltage or current through a generating electrode (GE) and counter-generating electrode (GE') [13]. Reactions occurring at the anode and cathode are as follows:

$$2H_2O \rightarrow 4H^+ + 4e^- + O_2 \quad \text{(at anode)} \qquad (1)$$

$$4H_2O + 4e^- \rightarrow 4OH^- + 2H_2 \text{ (at cathode)} \qquad (2)$$

Accumulation of these dissolved gas molecules at the generating electrode, in turn, rapidly establishes a microenvironment of oxygen saturation or hydrogen saturation. The accumulation and saturation of hydrogen molecules takes place after the depletion of oxygen. An oxygen microsensor in close proximity to the surrounded generating electrode can be confined in a controlled microenvironment. A two-point self-diagnostic procedure for the oxygen sensor can then be performed, with the high point diagnosis being established in an oxygen-saturated phase, and the low point diagnosis in an oxygen-depleted phase, respectively. These transient perturbations of the microenvironment are expected to equilibrate rapidly with the surrounding solution medium.

## III. METHODS

### 1. Device design

We designed and fabricated polarographic micro-oxygen sensors on flexible polyimide substrates (Kapton®). The basic electrochemical three electrode cell configuration was adopted to avoid the ohmic voltage drop through the electrolyte between the anode and cathode. All electrodes were designed to be

geometrically symmetric to assure diffusional mass transport of electrochemical species in all radial directions. The noise at an electrode-electrolyte interface can be modeled by two sources [14] - 1/f noise and white noise. The 1/f noise is inversely proportional to the electrode area. A lower form factor for the electrode (the circumference to surface area ratio) results in a lower white noise level, which implies that the noise generated by a circular type electrode is lower than any other type of electrodes. Therefore we used a circular working electrode (WE). The conventional Clark oxygen sensor contains a reference electrode (RE) and a working electrode located in the same compartment filled with an internal electrolyte gel which is encapsulated by a hydrophobic, electrically non-conducting membrane. To circumvent the technical difficulties of fabricating the reliable double-layered membrane (electrolyte gel/hydrophobic membrane) [15, 16], we did not use any membrane in this study.

Figure 2 shows the layout and cross section of the concentric type electrode configuration. The middle electrode serves as the working electrode at which dissolved oxygen molecules are cathodically reduced. The generating electrode is wrapped around the working electrode; this configuration will establish oxygen-saturated or oxygen-depleted microenvironments during self-diagnosis phases. Proceeding from inside to outside, the next concentric circle can be used as the reference electrode. The outermost electrode in Figure 2 is the counter electrode (CE) of this three-electrode cell. It is placed at a distance from the working electrode to minimize electrochemical interference of byproducts generated at the counter electrode. The counter-generating electrode, not shown, is located even more remotely from the working electrode for this same reason.

## 2. Microfabrication

All of the prototype sensors were fabricated in the facilities of the Biomedical Microsensors Laboratory (BMMSL) at North Carolina State University [17]. All electrodes were platinum as shown in Figure 2 (b). Conventional platinum lift-off processes are difficult to execute on Kapton® substrates when organic solvent-based photoresist chemistries are required. This is because the long immersion in the solvents required for lift-off tends to degrade the adhesion of the metal to the Kapton® substrate. On the

other hand, wet chemical etching of platinum in heated aqua regia, while common on glassy substrates, was unsuccessful on Kapton® substrates for undetermined reasons. Instead, the substrates were first metallized with chromium and gold, but these layers were left unpatterned until after the deposition and lift-off of the platinum electrodes. This sequence has the advantage that the chromium and gold layer protects the Kapton® substrate from contact with the solvents during titanium and platinum lift-off.

Flexible polyimide substrates (Kapton®, Du Pont, type VN, 75 μm in thickness), were cleaned in successive rinses of acetone, methanol, and deionized water, and then dehydrated at 120 °C. A thin film of chromium as an adhesion layer, followed by a 0.2 μm film of gold was deposited on the substrate by DC magnetron sputtering. Positive photoresist (Shipley 1813) was spin-coated, selectively exposed through the photomasks with broad band UV light, and developed to pattern the electrode features. After deposition by DC magnetron sputtering of a thin titanium film and a 0.08 μm platinum film, the whole substrate was agitated in acetone to lift-off the photoresist layer along with unwanted titanium and platinum. Positive photoresist (Shipley 1813) was spin-coated again to protect the platinum layer during wet etching of the uncovered gold and chromium layers. After removal of the photoresist with solvents (Shipley 1165), the substrate was cleaned with organic solvents and dehydrated in preparation for the application of the polyimide dielectric layer. Photosensitive polyimide (HD Microsystems, Pyralin PI-2723) was spin-coated to a nominal thickness of 2.0 μm and exposed in the same manner as the photoresist. Subseqent development and thermal curing of the polyimide defined the platinum electrodes.

The use of a polyimide (Kapton®) substrate, which can be implemented as a flexible planar microsensor array, provides unique advantages for this specific application especially in terms of immunity to motion artifacts. Metal patterning to 10 μm line width was achieved. Smaller line widths are possible, but are more difficult due to thermal expansion of the Kapton® substrate during the microfabrication process and surface roughness of the substrate. The electrochemical properties of each sensor from same wafer were showed some nonuniformity. In the future, we envision an optimized microfabrication process that includes more precise photolithography with higher resolution and the

supporting the flexible substrate during processing with a rigid wafer to minimize thermal instability and substrate roughness.

## 3. Measurements

The fabricated Kapton®-based oxygen microsensor was connected to the test instruments via a zero-insertion force (ZIF) connector and cable as shown in Figure 3. A commercial miniature reference electrode (Harvard Apparatus, AH69-0024) was used in this study in place of the on-chip reference electrode to avoid possible instability of thin film Ag/AgCl electrode caused by electrochemical crosstalk with hydrogen peroxide which is a byproduct of the reaction [18]. The sensor was placed in a measuring vessel and the solution was saturated with different oxygen/nitrogen gas ratios at room temperature. Oxygen tension in the bulk solution was monitored with a commercial oxygen meter (Instech, SYS203). All measurements were done in a stationary solution to prevent any solution convectional effects.

A custom set of electrochemical instrumentation has been employed. A potentiostat (Gamry Instruments, FAS1) and a galvanostat (Gamry Instruments, 750) were used to bias the 3-electrode oxygen microsensor and to operate the generating electrodes, respectively. These two modules were plugged into one control PC and operated in a floating-ground mode to prevent electrical interference between the two modules. The cathodic potential for oxygen reduction (-0.7 V vs. Ag/AgCl) was chosen from the plateau region in a traditional voltammogram. To control the microenvironment near the working electrode of the oxygen microsensor, constant currents were forced between the pair of generating and counter-generating electrodes. Figure 4 shows a schematic of the measurement system.

A script was written to perform two different procedures for the establishment of microenvironments. First, the operation of the system was divided into a generation phase and followed by a measurement phase (mode (a) in Figure 4). After a predefined gas-generating phase, the oxygen sensor was triggered by the potentiostat, which provides a potential step to the working electrode for oxygen reduction and then makes chronoamperometric measurements of the sensor's response. Any change in the microenvironment during the generating phase will affect transient response of the sensor.

This two-phase process helps eliminate any possible electrostatic coupling between the three-electrode oxygen microsensor and the generating electrode source. The second calibrating procedure involved a simultaneous gas-generating phase during sensor operation (mode (b) in Figure 4). By this procedure, monitoring of any changes in the microenvironment during the preceding generating phase is possible by comparing real-time measurements with the sensor's baseline response, which reflects the background oxygen content. After each measurement, the solution was equilibrated to a defined baseline value by bubbling with a fixed ratio of oxygen and nitrogen gases and magnetically stirring.

## IV. RESULTS AND DISCUSSION

### 1. Characterization of the working and generating electrodes

Every new device was pre-polarized for about 30 minutes at the cathodic potential for oxygen reduction (-0.7 V vs. Ag/AgCl) before the actual measurements to obtain stabilized values. Figure 5 shows typical chronoamperometric responses of the oxygen microsensor with a platinum working electrode in various bulk oxygen contents. Typical chronoamperometric responses are first observed at the onset of potential pulses to the working electrode. Afterwards the current reaches a steady-state value, which is called an oxygen limiting current. According to the limiting current theory, the relationship between limiting current magnitude and oxygen content is linear over the entire concentration range. The pH change during the oxygen reduction at the working electrode is considered to attribute to the nonlinearity of current magnitude versus oxygen content in Figure 5. It is known that the stoichiometric coefficient of oxygen reduction, between 2.0 and 4.0, depends on bulk solution pH [19]. Oxygen reduction occurs predominantly in a single 4-electron step at low bulk solution pH:

$$O_2 + 2H_2O + 4e^- \rightarrow 4OH^- \qquad (3)$$

And an increase in bulk pH increases the proportion of two-electron step:

$$O_2 + 2H_2O + 2e^- \rightarrow H_2O_2 + 2OH^-, \quad H_2O_2 + 2e^- \rightarrow 2OH^- \qquad (4)$$

As the oxygen concentration increases, the decrease in pH change at the surface of the working electrode (i.e. the accumulation of $OH^-$ ions) becomes more significant to reduce the stoichiometric coefficient. Other factors that influence this coefficient, such as electrode material, reduction potential, surface aging and pretreatment, remained the same in this study.

Figure 6 shows a cyclic voltammogram of a platinum generating electrode in an air-saturated phosphate buffer solution (10 mM, pH 7.4). Oxygen and hydrogen peaks can be seen at the right and left edges of the water electrolysis window, respectively. The minimum generating current was chosen to be 49 nA (0.5 $mA/cm^2$) for oxygen generation and – 147 nA (– 1.5 $mA/cm^2$) for oxygen depletion, respectively, to ensure high current efficiency for water electrolysis during the establishment of the microenvironments. Selecting a generating electrode material with a narrower water electrolysis window will have benefits for this application by maximizing the current efficiency for electrolyzing water and minimizing the power consumption.

2. Transient response preceded by a separate generating phase

Constant generating currents were driven through the generating (anode) and counter-generating electrodes (cathode) for up to 90 seconds to establish a stable microenvironment around the working electrode. Transient chronoamperometric responses in an air-saturated solution were recorded immediately following the generating phase as described in Figure 4 (a). As the duration of generating current pulses increases, the magnitudes of initial transient response increase as shown in Figure 7 (a). This means that a steady-state oxygen-rich environment has been established in the vicinity of the sensor as expected since a larger number of oxygen molecules were generated by the longer current durations. Convergence of all curves to bulk oxygen value (response to the air-saturated solution) means that the oxygen-rich environment is being equilibrated with the surrounding medium. With a generating current density of 5 $mA/cm^2$ the effect of generating current durations of longer than 30 seconds was about the same, suggesting that the degree of oxygen accumulation around the sensor in the generating phase reaches steady-state after about 30 seconds. Shortly after the completion of these measurements in the air-

saturated environment, the solution was saturated with 100 % oxygen to compare the sensor response. Note that the initial peaks after the generation phase in the air-saturated solution approach that obtained in the oxygen-saturated solution. A similar procedure was then applied to observe the transient response of the sensor after an oxygen-depleting phase provided by reversing the current direction through the generating electrode. Figure 7 (b) shows typical responses of another sensor from the same wafer. The response after the depleting phase shows a reduced initial height followed by a recovery to the bulk response.

The main factors governing this microenvironment are the diffusion coefficient and mobility of the generated molecules (dissolved gases, hydrogen and hydroxyl ions) in the sample solution. These electrochemical parameters will be affected by the solution composition. Also the electrode kinetics (oxygen reduction at the working electrode, redox processes for oxygen/hydrogen generation, and hydrogen/hydroxyl ion production at the generating electrode) may be affected by electrochemical interference of species in the sample solution. Sensor geometry, especially the spacing between working and generating electrodes, will be the predominant parameter to determine the optimum conditions to control the microenvironment, which is a critical element in the performance of the *in situ* self-diagnosis sensor. A small electrode area and close spacing between the electrodes is required to reduce the overall sensor size and to minimize oxygen consumption by the sensor itself. The sensor's geometric structure should be optimized to minimize the duration and magnitude of the generating signal.

3. Quasi steady-state response during a simultaneous generating phase

The generating phase was performed during the normal operation of the sensor for the mode of operation described in Figure 4 (b). Once the limiting current condition at a given bulk oxygen content had been achieved after application of the oxygen reduction potential to the sensor, the generating current were applied to the generating electrode for 90 seconds. The limiting current level (the baseline during the response) reflects the bulk oxygen content around the sensor. Various time responses during the generating phase are shown in Figure 8 (a). Simultaneous operation of the potentiostatic instrument (for

biasing the oxygen microsensor) and the galvanostatic instrument (for driving the generating current) produced a quasi steady-state response during the generating phase. For comparison the response to oxygen-saturation was recorded shortly after the completion of these measurements in the air-saturated case in the same solution. It can be seen that the responses during each generating phase approaches the limiting current levels of the oxygen-saturated solution and then gradually returns to the original level of bulk oxygen content. As the generating current density increases the corresponding response increases, which agrees with the result shown in Figure 7 (a). With the current density higher than 16 $mA/cm^2$, tarnish on the generating electrode surface and damage to the polyimide encapsulation were observed occasionally in some of the devices.

At a given temperature, the limiting current magnitude in the oxygen-saturated solution (100% oxygen-saturation) is limited to 4.76 times of that in the air-saturated solution (21% oxygen-saturation) at 1 atm. During the generating phase with higher generating current densities, however, responses exceeding this limit were observed. The most plausible explanation for this is the supersaturation of the electrochemically generated oxygen in the microenvironment covering the working electrode [20]. The concentration of the electrochemically generated oxygen near the oxygen-evolving anode surface can exceed the standard oxygen solubility in water at 1 atm without the formation of gas bubbles. The pH change in the microenvironments due to water electrolysis is also expected to have contributed to this exaggerated response. The generation of dissolved oxygen and hydrogen is accompanied by a pH shift at the electrode surface as shown in equations (1) and (2), which means the microenvironment will undergo pH changes during the generating phases. Subsequently, the oxygen catalytic activity of the platinum working electrode should be enhanced by the lower pH induced in the microenvironment according to equation (3) during this phase.

To observe the overall influence of pH and supersaturation, the generating phase was performed in an oxygen-saturated solution. The lower curve in Figure 8 (b) is a plot of the percent changes of response during the oxygen-generating phase with respect to the baseline at the oxygen-saturated solution. At the highest current density the response was almost doubled from the baseline (response to the oxygen-

saturated solution), suggesting that either the stoichiometric coefficient was increased or supersaturation was established, or both. To further investigate the influence of the pH changes during the oxygen-generating phase, measurements were performed in solutions with different pH buffering capacities. The response magnitudes in a 1 mM buffer solution were most pronounced, which implies that in stronger buffer solutions the pH changes were suppressed to minimize the perturbation of the stoichiometric coefficient of oxygen reduction. At the highest current density, the responses during the generating phase were similar with the oxygen-saturation value (theoretically 476%) in 10 mM and 100 mM buffer solution. This suggests that an *in situ* high-point calibration (100% oxygen) can be accomplished by establishing an oxygen-saturated microenvironment with a refined device structure and generating signal.

Other factors may have contributed to the exaggerated responses; first, a considerable concentration-driven convection by the oxygen molecules diffusing from the generating electrode could enhance the mass transport of oxygen in the stagnant solution, thereby increasing the limiting current value of the oxygen-saturated solution. A second factor may be "feedback" of electrochemically generated oxygen generated from hydrogen peroxide [18], a byproduct of oxygen reduction at the working electrode as in equation (4). Hydrogen peroxide is being oxidized to oxygen at the anodic generating electrode and contributes to the oxygen-rich microenvironment.

$$H_2O_2 \rightarrow 2H^+ + O_2 + 2e^- \qquad (5)$$

Thirdly, the possibility of temperature elevation around the microsensor due to high current densities. The generation of gas bubble has not been monitored during this study. Further analysis of these factors is necessary to adapt the proposed system for practical applications.

The effect of stirring on the microenvironment was also investigated. As expected, the magnitude of response diminished with energetic stirring of the solution as in Figure 8 (c). The response of the same sensor without solution stirring is given for comparison. Note the increased baseline produced by stirring. This result allows us to ascertain that the contribution of electrical interference to the response by the potentiostat operating the oxygen microsensor and the galvanostat operating the generating electrode pair is negligible.

Figure 9 (a) shows the quasi-steady state responses during the oxygen-depleting phase. Analogous to the generating phase, the sensor responses during depleting phases approach the limiting current levels at nitrogen-saturation, followed by a return to the original level of bulk oxygen content. As the current density increases the corresponding response decreases, which is consistent with Figure 7 (b). It should be noted from Figure 9 (b) that the responses with the current density higher than 5 $mA/cm^2$ remains around 30 % of the bulk response without significant decrease beyond this level. This implies that the oxygen depletion has not been completely accomplished with the given electrode geometry over the entire current density range. The higher pH in the microenvironment during the depleting phase is assumed to further decrease the sensor response due to the reduction of catalytic activity of the working electrode to reduce oxygen. Improvements in sensor structure are expected to achieve a low-point *in situ* calibration during the sensor operation.

Incorporation of a Clark type microsensor structure should minimize the pH effects and possible electrical interference caused by the galvanostat. By encapsulating a 3-electrode oxygen sensor within a double-layer gas permeable membrane, consisting of an outer hydrophobic and an inner hydrophilic layer, the oxygen sensor itself can be fully isolated from the surrounding generating electrode. However, microfabrication of a reliable and repeatable double-layered polymeric structure is challenging. In addition, lower oxygen permeability with the double-layer membrane will cause longer response time and will require a higher amplitude and longer duration of the generating signal.

## VI. CONCLUSION

The concept of an *in situ* self-diagnostic technique for a dissolved oxygen microsensor is proposed in an effort to devise an intelligent microsensor system with an integrated electrochemical actuation electrode. The feasibility of the proposed concept is demonstrated in a physiological solution. The sensor responds properly during both the oxygen-generating and oxygen-depleting phases. The integrated electrochemical actuator is a useful tool for achieving built-in intelligence of the dissolved

oxygen microsensor. The results suggest that the use of these microenvironments for *in situ* self-diagnosis and *in situ* self-calibration can be expected with carefully refined microstructures and generating signals. This intelligent capability of oxygen microsensors is needed to improve their reliability during their *in situ*, and potentially *in vivo*, operation.

## ACKNOWLEDGEMENTS

This research was supported partly by a grant from the NASA Office of Biological and Physical Research (01-OBPR-01), and by Sicel Technologies, Inc., Research Triangle Park, North Carolina.

## REFERENCES

1. B. H. van der Schoot and P. Bergveld, "An ISFET-based microlitre titrator: integration of a chemical sensor-actuator system," Sensors and Actuators, Vol. 8, pp. 11-22, 1985.
2. B. H. van der Schoot and P. Bergveld, "Coulometric sensors: the application of a sensor-actuator system for long-term stability in chemical sensing," Sensors and Actuators, Vol. 13, pp. 251-262, 1988.
3. B. K. Sohn and C. S. Kim, "A new pH-ISFET based dissolved oxygen sensor by employing electrolysis of oxygen," Sensors and Actuators B-Chemical, Vol. 34, pp. 435-440, 1996.
4. M. Lehmann, W. Baumann, M. Brischwein, H. J. Gahle, I. Freund, R. Ehret, S. Drechsler, H. Palzer, M. Kleintges, U. Sieben, B. Wolf, "Simultaneous measurement of cellular respiration and acidification with a single CMOS ISFET," Biosensors and Bioelectronics, Vol. 16, No. 3, pp. 195-203, 2001.
5. J. Hendrikse, W. Olthuis and P. Bergveld, "The $^{E}$MOSFET as an oxygen sensor: constant current Potentiometry," Sensors and Actuators B-Chemical, Vol. 59, pp. 35-41, 1999.

6. T. W. A. Dam, W. Olthuis and P. Bergveld, "Electroactive gate materials for a hydrogen peroxide sensitive $^{E}$MOSFET," IEEE Sensors Journal, Vol. 2, pp. 26-33, 2002.
7. J. Wu and W. Sansen, "Electrochemical time of flight flow sensor," Sensors and Actuators B-Chemical, Vol. 97-98, pp. 68-74, 2002.
8. A. Poghossian, J. W. Schultze and M. J. Schoning, "Multi-parameter detection of (bio-)chemical and physical quantities using an identical transducer principle, Sensors and Actuators B-Chemical, Vol. 91, No. 1-3, pp. 83-91, 2003.
9. B. H. van der Schoot, H. Voorthuyzen and P. Bergveld, "pH-static enzyme sensor. Design of the pH control system," Sensors and Actuators B-Chemical, Vol. 1, No. 1-6, pp. 546-549, 1990.
10. H. I. Seo, C. S. Kim, B. K. Sohn, T. Yeow, M. T. Son and M. Haskard, "ISFET glucose sensor based on a new principle using the electrolysis of hydrogen peroxide," Sensors and Actuators B-Chemical, Vol. 40, pp. 1-5, 1997.
11. F. Kreuzer, H. Kimmich, M. Brezina and J. Heyrovsky, "Polarographic determination of oxygen in biological materials," in J. Koryta (ed.), *Medical and biological applications of electrochemical devices*. John Wiley & Son, 1980, pp. 173-261.
12. I. Fatt, *The polarographic oxygen sensor: its theory of operation and its application in biology, medicine, and technology,* CRC Press, 1976.
13. C. S. Kim, J. O. Fiering, C. W. Scarantino and H. T. Nagle, "A novel in situ self-calibration method for an oxygen microsensor," World Congress on Medical Physics and Biomedical Engineering, Abstract No. WE-Ba205-02 (CD-ROM), Chicago, USA, 2000.
14. M. Lambrechts and W. Sansen, *Biosensors: microelectrochemical devices,* IOP Publishing, 1992, pp. 206-208.
15. G. Jobst, G. Urban, A. Jachimowicz, F. Kohl, O. Tilado, I. Letternbichler and G. Nauer, "Thin-film Clark-type oxygen sensor based on novel polymer membrane systems for in vivo and biosensor applications," Biosensors and Bioelectronics, Vol. 8, pp. 123-128, 1993.

16. Ph. Arquint, A. van den Berg, B. H. van der Schoot, N. F. de Rooij, H. Buhler, W. E. Morf and L. F. J. Durselen, "Integrated blood-gas sensor for $pO_2$, $pCO_2$ and pH," Sensors and Actuators B-Chemical, Vol. 13-14, pp. 340-344, 1993.

17. R. P. Buck, V. V. Cosofret, E. Lindner, S. Ufer, M. B. Madaras, T. A. Johnson, R. B. Ash and M. R. Neuman, "Microfabrication technology of flexible membrane-based sensors for in-vivo applications," Electroanalysis, Vol. 7, pp. 846-851, 1995.

18. C. S. Cha, M. J. Shao and C. C. Liu, "Problems associated with the miniaturization of a voltammetric oxygen sensor: chemical crosstalk among electrodes," Sensors and Actuators B-Chemical, Vol. 2, pp. 239-242, 1990.

19. V. Linek, V. Vacek, J. Sinkule and P. Benes, *Measurement of Oxygen by Membrane-covered Probes*, Ellis Horwood, 1988. pp. 17-24.

20. S. Bohm, W. Olthius and P. Bergveld, "An integrated micromachined electrochemical pump and dosing system," Journal of Biomedical Microdevices, Vol. 1, No. 2, pp. 121-130, 1999.

FIGURE CAPTIONS

**Figure 1.** Concept for a novel oxygen sensor with *in situ* self-diagnosis capability. The microenvironment is generated by a generating electrode (GE) which surrounds the microsensor. Oxygen-saturated or oxygen-depleted phases can be established by water electrolysis depending on the polarity.

**Figure 2.** Concentric 3-electrode oxygen sensor with total diameter of 200 micron meter, (a) Layout of exposed electrodes (not to scale), (b) cross-sectional view after fabrication on a flexible Kapton® substrate (1. substrate cleaning, 2. Au/Cr deposition, 3. Pt/Ti deposition, 4. Pt/Ti lift-off, 5. Au/Cr etching, 6. polyimide patterning).

**Figure 3.** Photograph of a probe assembly. An oxygen microsensor fabricated on flexible Kapton® substrate (upper right part) is connected to a ribbon cable via a zero-insertion force (ZIF) connector (lower part).

**Figure 4.** Measurement scheme. A potentiostat and a galvanostat are employed for biasing the 3-electrode oxygen microsensor and for generating microenvironments, respectively, (a) Sequential generating mode for transient response, (b) Simultaneous generating mode for quasi steady-state response.

**Figure 5.** Time responses (chronoamperometry) of the oxygen reduction current at a Pt working electrode responding to potential step (-0.7 V vs. Ag/AgCl) in phosphate buffer solution (pH 7.4, 10 mM) with various oxygen contents.

**Figure 6.** Voltammogram of a Pt generating electrode in air-saturated phosphate buffer solution (pH 7.4, 10 mM, scan rate: 50 mV/sec).

**Figure 7.** Typical transient responses after an initial generating phase in air-saturated phosphate buffer solution (pH 7.4, 10 mM), (a) effect of oxygen-generating phase with current pulses (5 $mA/cm^2$) on the generating electrode with various durations, with a sensor response to oxygen-saturated solution for comparison, (b) effect of oxygen-depleting phase with current pulses (same pulse in the opposite polarity) on the generating electrode with various durations, with a sensor response to nitrogen-saturated solution for comparison.

**Figure 8.** Typical quasi steady-state responses during the simultaneous oxygen-generating phase, (a) effect of the oxygen-generating phase with various current densities in air-saturated phosphate buffer solution (pH 7.4, 10 mM), with a sensor response to oxygen-saturated solution for comparison, (b) percent changes in the sensor responses (ratio of the steady-state value at t=90 with respect to the baseline at t=0) according to the generating current density in various pH buffering capacities, with those in an oxygen-saturated solution for comparison, (c) effect of vigorous solution stirring in air-saturated phosphate buffer solution (pH 7.4, 10 mM), with a sensor response to a stationary solution for comparison.

**Figure 9.** Typical quasi steady-state responses during the simultaneous oxygen-depleting phase in air-saturated phosphate buffer solution (pH 7.4, 10 mM), (a) effect of the oxygen-depleting phase with various current densities, with a sensor response to nitrogen-saturated solution for comparison, (b) percent changes in the sensor responses (ratio of the steady-state value at t=90 with respect to the baseline at t=0) according to the generating current density.

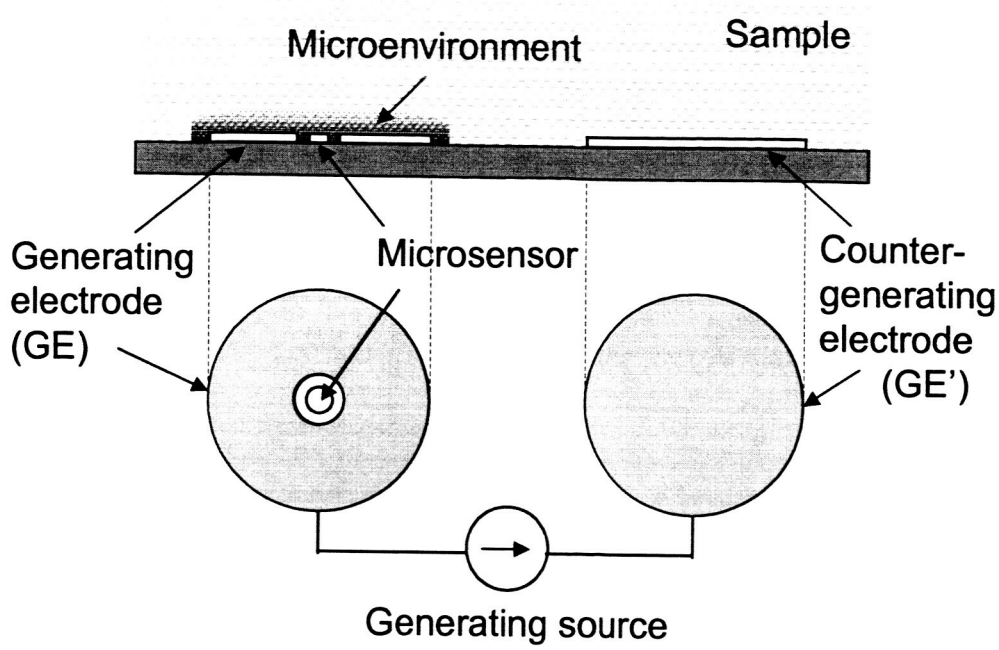


Figure 1.

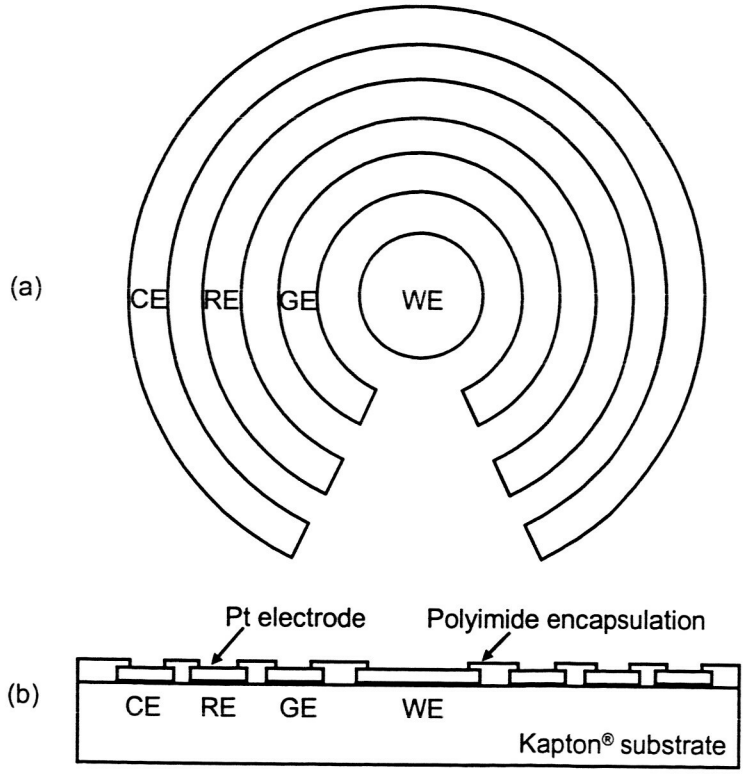


Figure 2.

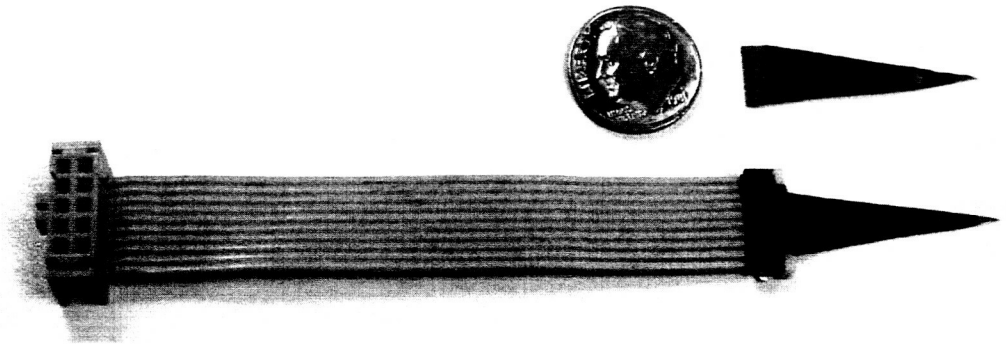

Figure 3.

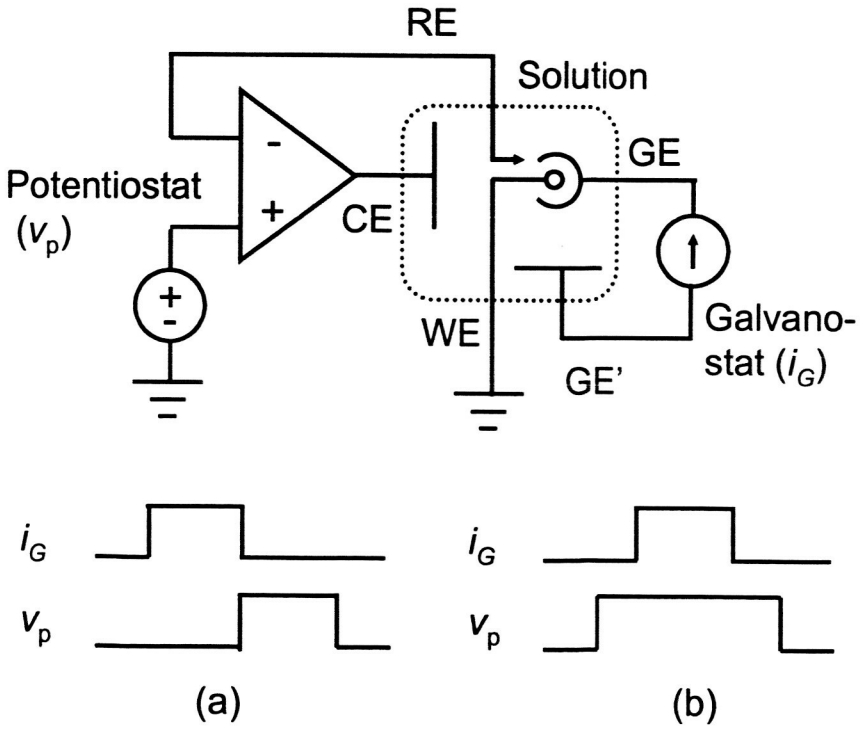


Figure 4.

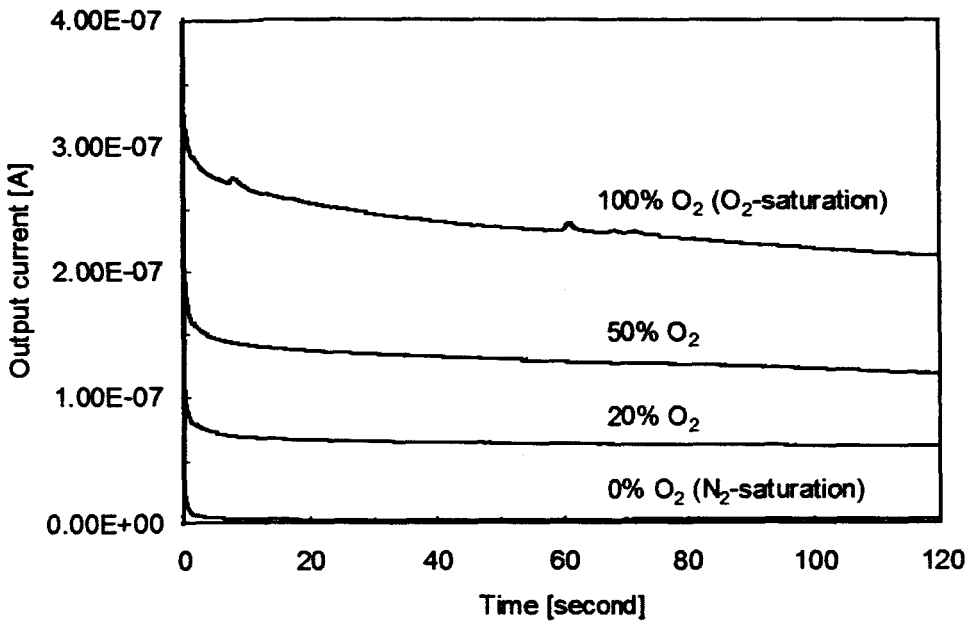


Figure 5.

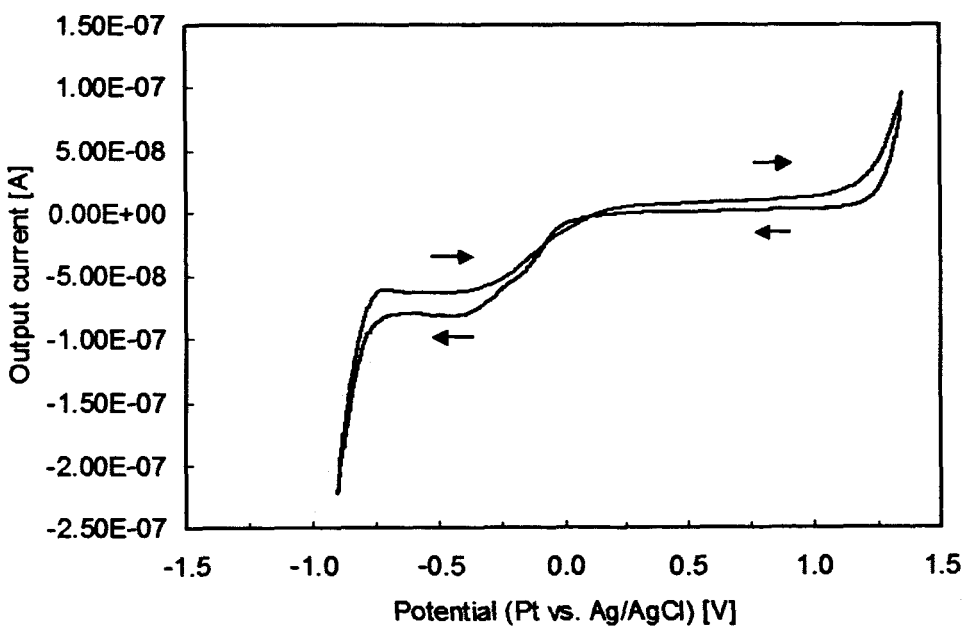


Figure 6.

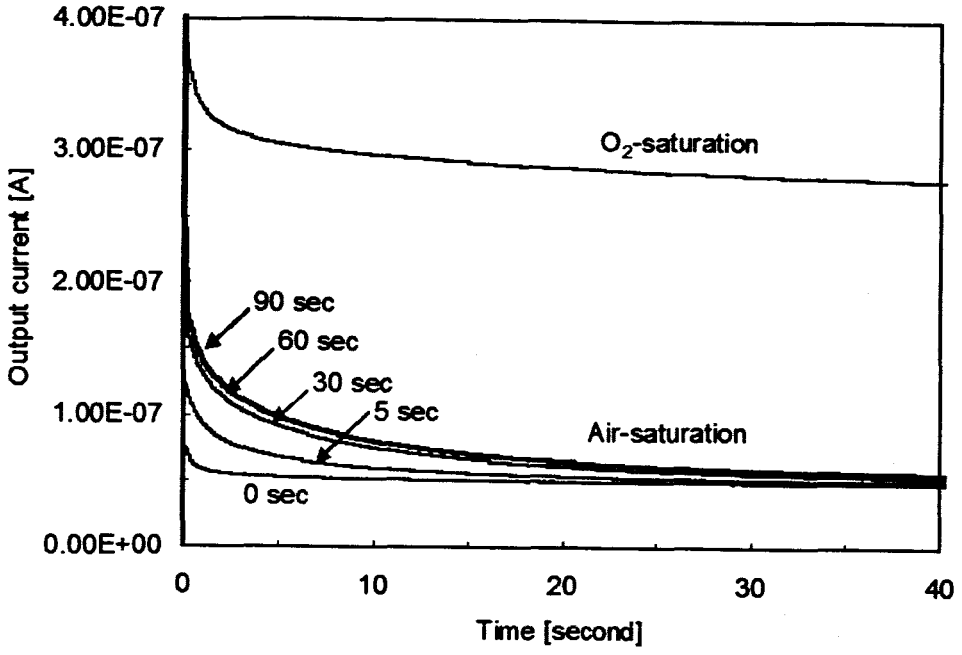


(a)

Figure 7 (a).

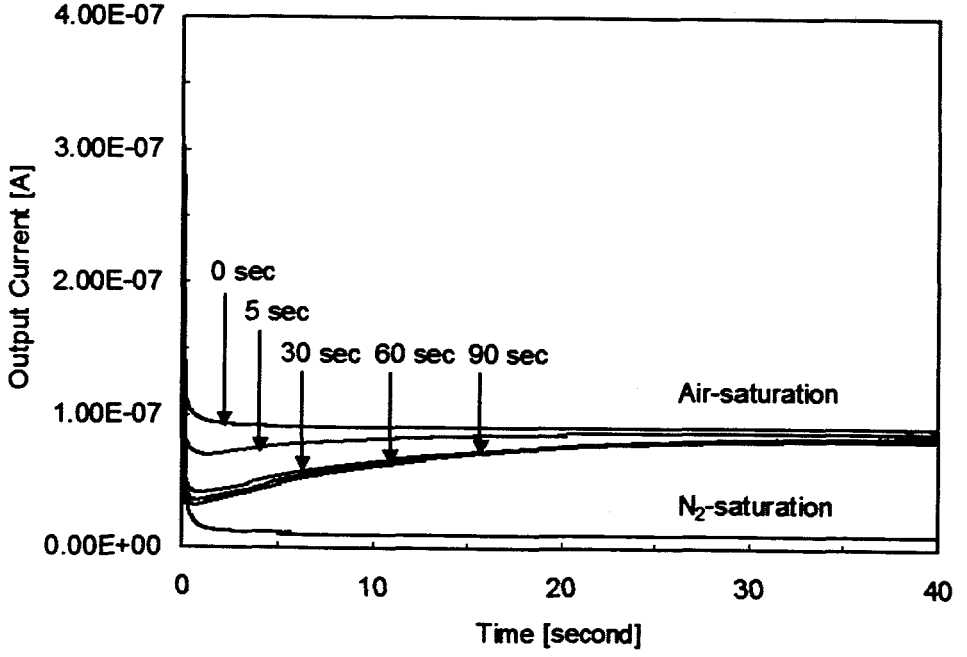


(b)

Figure 7 (b).

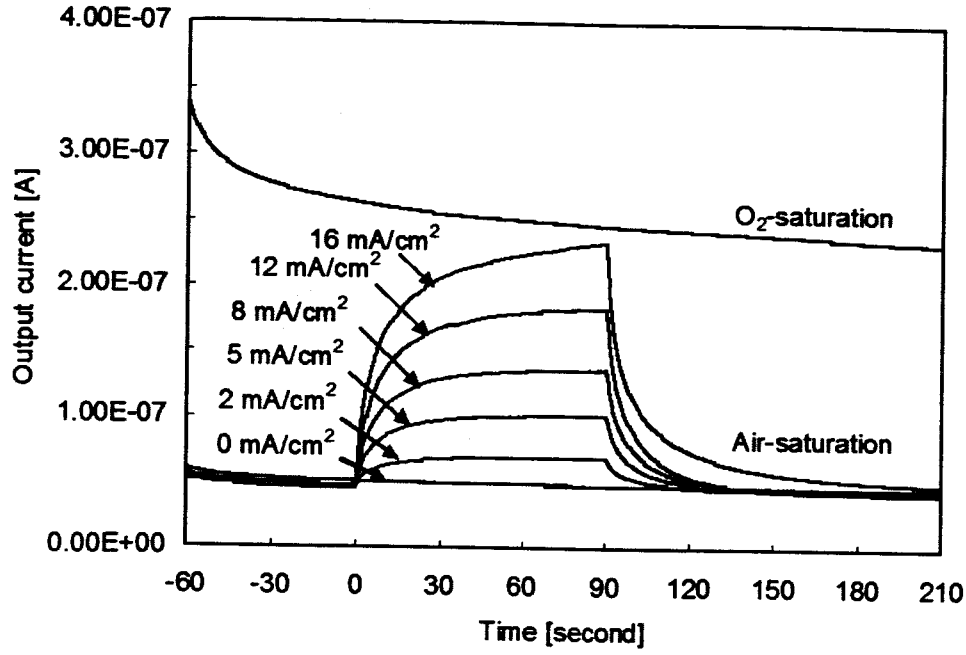


(a)

Figure 8 (a).

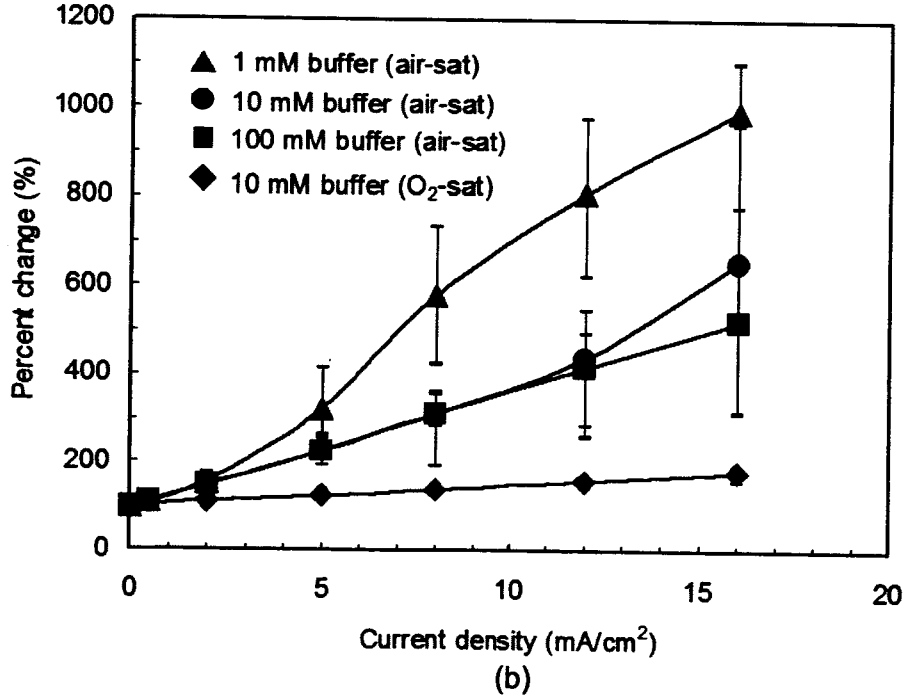


(b)

Figure 8 (b).

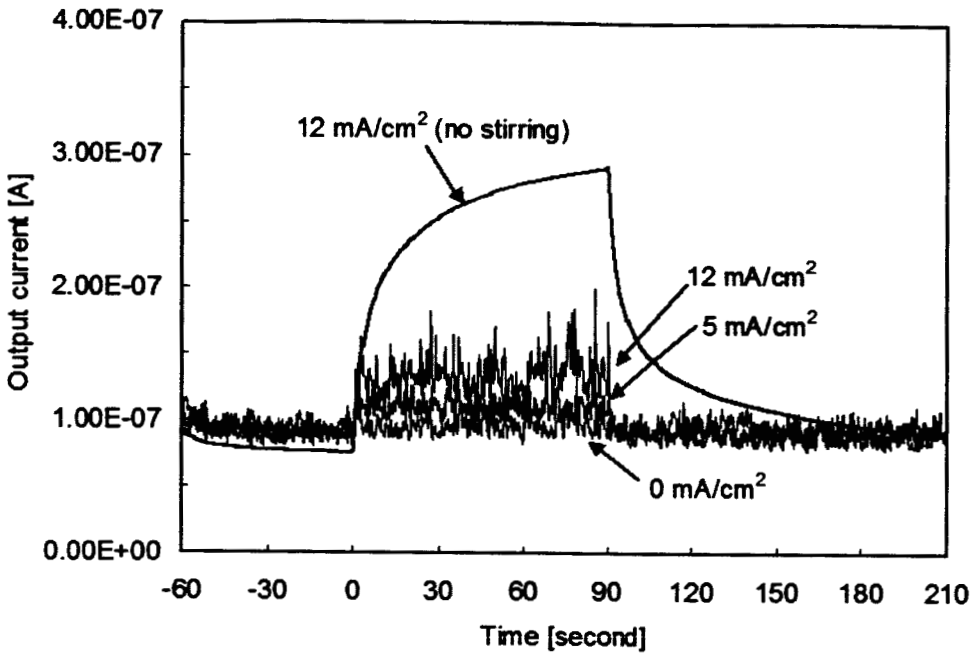
4.00E-07
3.00E-07
2.00E-07
1.00E-07
0.00E+00
Output current [A]
12 mA/cm2 (no stirring)
12 mA/cm2
5 mA/cm2
0 mA/cm2
-60
-30
0
30
60
90
120
150
180
210
Time [second]

(c)

Figure 8 (c).

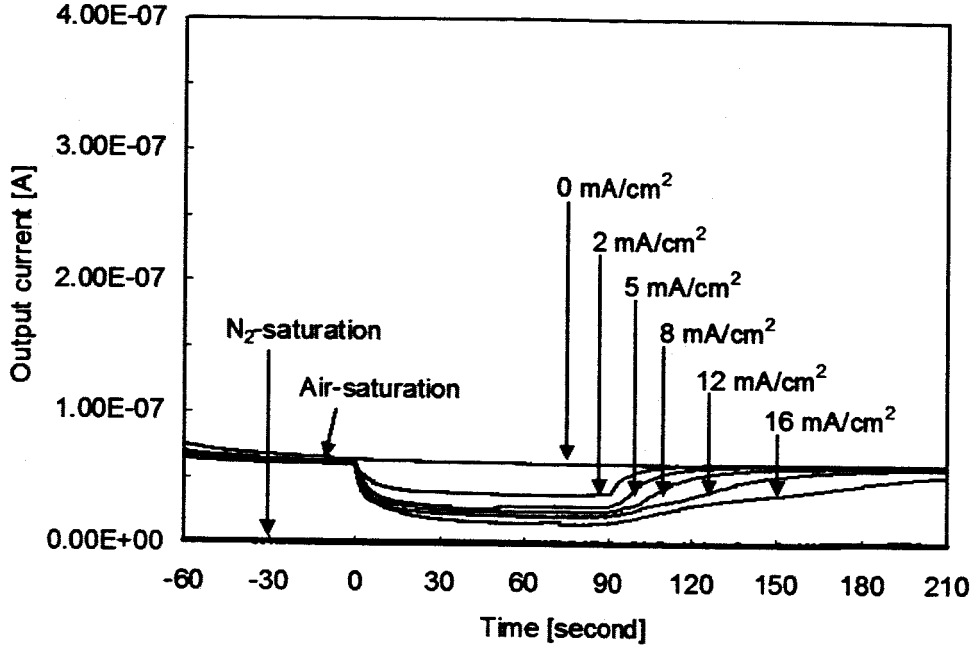


(a)

Figure 9 (a).

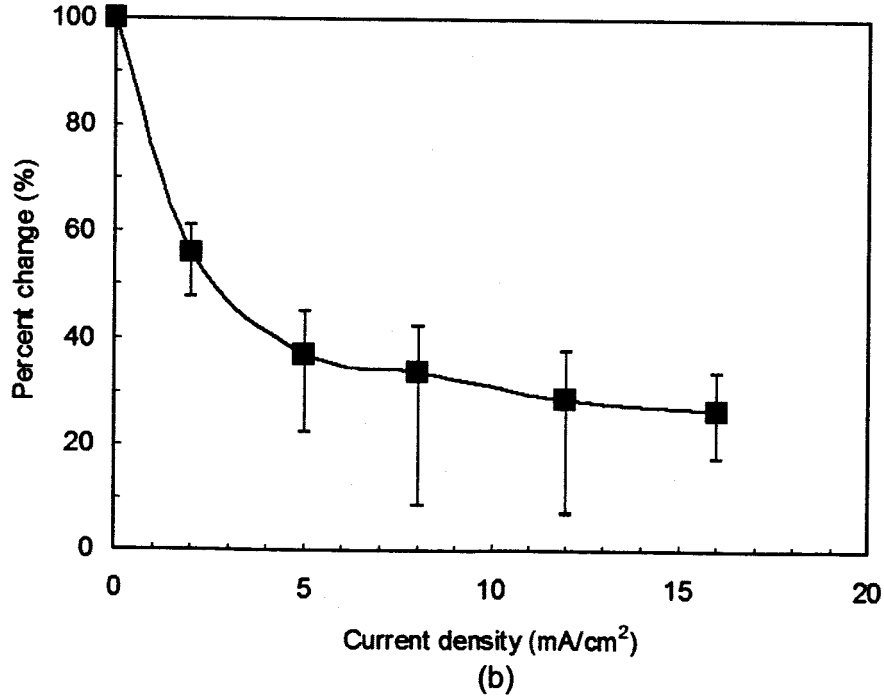


(b)

Figure 9 (b).

## Appendix 2 (article to be submitted to Habitation Journal or equivalent)

# Flexible Microsensor Array for the Root Zone Monitoring of Porous Tube Plant Growth System

**Sandeep Sathyan, D. Marshall Porterfield, H. Troy Nagle, Christopher S. Brown, Chang-Soo Kim***

Sandeep Sathyan, Chang-Soo Kim*: Departments of Electrical and Computer Engineering and Biological Sciences, University of Missouri-Rolla, Rolla, MO 65409, USA. 573-341-4529 (voice), 573-341-4532 (fax), ss6x7@umr.edu, ckim@umr.edu

D. Marshall Porterfield: Departments of Biological Sciences and Electrical and Computer Engineering, University of Missouri-Rolla, Rolla, MO 65409, USA. 573-341-6336 (voice), 573-341-4821 (fax), mporterf@umr.edu

H. Troy Nagle: Biomedical MicroSensors Laboratory, Department of Electrical and Computer Engineering, North Carolina State University, Raleigh, NC 27695-7911, USA, 919-515-3578 (voice), 919-513-3814 (fax), t.nagle@ncsu.edu

Christopher S. Brown: Kenan Institute for Eng., Tech., & Science, North Carolina State Univ., USA. 919-515-5118 (voice), 919-515-5831 (fax), cbrown@ncsu.edu

* Corresponding author

**ABSTRACT**

Control of oxygen and water in the root zone is vital to support plant growth in the microgravity environment. The ability to control these sometimes opposing parameters in the root zone is dependent upon the availability of sensors to detect these elements and provide feedback for control systems. In the present study we demonstrate the feasibility of using microsensor arrays on a flexible substrate for dissolved oxygen detection, and a 4-point impedance microprobe for surface wetness detection on the surface of a porous tube (PT) nutrient delivery system. The oxygen microsensor reported surface oxygen concentrations that correlated with the oxygen concentrations of the solution inside the PT when operated at positive pressures. At negative pressures the microsensor shows convergence to zero saturation (2.2 μmol/L) values due to inadequate water film formation on porous tube surface. The 4-point microprobe is useful as a wetness detector as it provides a clear differentiation between dry and wet surfaces. The unique features of the dissolved oxygen microsensor array and 4-point microprobe include small and simple design, flexibility and multipoint sensing. The demonstrated technology is anticipated to provide low cost, and highly reliable sensor feedback monitoring plant growth nutrient delivery systems in both terrestrial and microgravity environments.

**Keywords – Dissolved oxygen microsensor, porous tube, plant nutrient solution delivery, conductivity, polyimide.**

## I. INTRODUCTION

In space farming, plants can effectively provide food and recycle air, wastes and water to support long-term manned exploration [1]. Currently the most challenging aspects of supporting plant growth in microgravity environments are controlling water, mineral nutrients, and oxygen bioavailability in the root zone and rhizosphere. An important aspect of this system to consider is we do know that water content and oxygen are inversely opposed due to chemical and physical limitations associated with oxygen in the liquid phase. Also the performance of the nutrient delivery system in microgravity may be altered as forces such as surface tension, atmospheric pressure and capillary action would come to dominate the system in the partial or complete absence of gravity [1, 2]. As a result of this space based experiments have demonstrated that microgravity conditions cause biophysical limitations leading to hypoxia in plant roots [3, 4]. Additionally, buoyancy driven convection is inhibited in microgravity, and this would functionally limit oxygen and dissolved solute transport to the relatively slow process of diffusional flux to provide gas exchange for metabolism. Due to these problems passive, open loop control of plant nutrient delivery subsystems are not adequate and instead active systems for the delivery of oxygen, water and nutrients are required. Closed loop controls, driven by sensor inputs will also be required as water and gas content of the rootzone are inversely related and require careful balance in order to insure optimized performance.

One of the critical operational requirements of a plant nutrient delivery system in microgravity is to provide effective fluid delivery system while preventing free liquid release into the cabin where it might be lost or damage other equipment [5]. As a result of this requirement plant nutrient delivery modules are effectively sealed. While this does not impede the systems effective ability to provide a uniform distribution of water and nutrients within the root zone it is another limiting design factor that might impact our ability to maintain adequate oxygen levels. Some engineers and biologists have considered this and designed passive nutrient delivery systems that allow for maintenance of water under controlled conditions, but these passive systems do not necessarily address biophysical problems with delivery of metabolic gasses to the root tissue [6]. Advanced active hydroponic systems have been proposed and developed, and one system that is being tested is the hydroponic porous tube plant nutrient delivery system as shown in figure 1 [7, 8, 9]. This porous tube provides efficient capillary interface between plant nutrient

solution and plant roots allowing provision of adequate levels of water and nutrients to the root zone [10, 11]. Precise monitoring and control of these parameters are required to avoid oxygen deficiency or insufficient aeration in the root zone area. To achieve this, advanced sensors having features such as small size, reliability, robustness, flexibility, easy calibration and biocompatibility have to be developed to provide exceptional benefits when used in plant growth system.

Other works by engineers and scientists have been directed at the development of advanced sensors for use in control of plant nutrient delivery systems. For example the Water Availability Sensor (WAS) was designed to measure water thickness on a PT surface based on infrared principles [2]. Other water sensors have been used based on resistance measurements [5] and also changes in thermal capacitance and thermal conductance [12]. These sensors were designed to meet some of the requirements of ideal sensors but only did so with limited success. Recent trends in sensor technology are based on the development of multifunctional and multipoint sensors that can be incorporated as on-chip intelligent and integrated sensors. Due to bulky and rigid designs the earlier sensors are incompatible and cannot be used as smart sensors incorporated on-chip, for small localized measurements.

Very few studies involving plant growth have shown the utilization of dissolved oxygen sensors for determining root zone activity. Commercially available Clark type and Whalen type electrodes are designed to be stir insensitive and sensitive only to diffusion based oxygen transport [13]. They have a hydrophobic membrane applied over the cathode. This ensures that the oxygen consumption in the electrode does not effect the oxygen concentration in the medium being measured. What this means is in microgravity, standard oxygen concentration sensors cannot be used as it cannot detect oxygen changes in non-diffusion based transport. The only way they can appropriately be used is where exact placement of the sensor and standardization of the system would be possible, in order to insure proper control feedback. Given the fact that amperometric oxygen sensors are fragile and/or bulky there use in these situations would be limited. A novel approach to this problem is the development of a biomimetic Root Oxygen Bioavailability (ROB) sensor, which has been used to directly measure changes in oxygen bioavailability in microgravity, when oxygen concentrations were constant [4]. For the present work our sensor was developed based on a flexible amperometric microsensor array. The sensor functions through the electrochemical reduction of oxygen and is flexible, miniature and robust in order to be used for direct measurement of oxygen concentrations on the surface of a PT. This array also includes a 4-point conductivity microprobe for wetness detection on the surface of porous tube plant nutrient delivery system. With its unique features (small and simple

structure, flexibility and multipoint sensing), the 4-point microprobe and dissolved oxygen microsensor array can be used to measure oxygen concentrations under standardized conditions that would not be possible with other electrochemical oxygen sensors.

## II. METHODS

### 1. Microsensor preparation

We designed an amperometric dissolved oxygen sensor based on the 3-electrode electrochemical cell configuration and a conductivity probe based on the 4-point impedance cell configuration. The 3-electrode cell minimizes the ohmic voltage drop through the electrolyte between the anode and cathode and prevents the consumption of reference electrode material (usually Ag/AgCl) [14]. Our electrochemical cell design, as in figure 2(a), comprises of concentric electrodes to ensure symmetric diffusional mass transport of electrochemical species in all radial directions. The center electrode serves as the reference electrode (RE) with an exposed diameter of 100 μm . Proceeding from inside to outside, the next concentric circle is used as the working electrode (WE). This is the site at which dissolved oxygen molecules are cathodically reduced. The outermost circle is the counter electrode (CE). The working electrode and counter electrode have a width of 50 μm each with their exposed surface areas being 3.8E-04 $cm^2$ and 7.6E-04 $cm^2$, respectively. The spacing between two successive concentric electrodes is 100 μm. The overall microsensor has a diameter 0.9 mm. The dissolved oxygen sensor strip made of flexible polyimide substrate consists of 4 microsensors as in figure 2(b). The strip is 58 mm long and 6 mm wide. This length enables the placement of sensors at equidistance of 10 mm when they are enwrapped on the porous tube surface. The 4-point conductivity sensor strip consists of 4 identical electrodes of diameter 500 μm with the outer pair of electrodes acting as current probes and the inner pair acting as voltage probes, respectively. The spacings between the current probes and the voltage probes are 80 mm and 76 mm, respectively.

All of the prototype sensors were fabricated in the facilities of the Biomedical Microsensors Laboratory (BMMSL) at North Carolina State University [15]. All the electrodes are made of platinum. On the Kapton® (polyimide) substrate, a thin film of chromium as an adhesion layer was first deposited. Platinum was deposited subsequently on the chromium layer. The metal layers were defined by conventional photolithography process. Then photosensitive polyimide was spin-coated and developed to encapsulate the platinum electrodes. Electroplating of Ag/AgCl on the reference electrode was carried out in a two step process. The first step involves silver plating on

platinum electrode with 1 wt% $KAg(CN)_2$ (1 g in 99 ml $H_2O$) as the plating solution. A constant current source (Keithley 225) was used to generate a constant current density of 0.25 $mA/cm^2$ for 10 minutes. The plating solution was magnetically stirred for uniform silver electroplating. In the second step, chloridation is achieved over the electroplated silver layer using 0.1 M NaCl as electrolyte with a current density of 0.25 $mA/cm^2$ for 3 minutes. For both the steps, platinum wire was used as counter electrode. The fabricated sensor was coated with poly-HEMA (poly 2-hydroxyethyl methacrylate), a hydrophilic membrane, by dipping method. This layer reduces stir sensitivity and acts as a protective membrane.

2. Setup

The plant nutrient delivery system shown in figure 3 includes a 1 liter liquid reservoir to store the plant nutrient solution. A gear pump (Cole Parmer, 7521-50) is utilized to draw out the solution from the reservoir and into the alumina porous tube (Refractron, porosity 0.5 μm, outer diameter 13 mm, inner diameter 8 mm, length 100 mm) at a constant flow rate of 15 ml/min. The internal pressure of the tube can be either positive or negative depending on the polarity of the pump direction. A valve on each side of the tube controlled the internal pressure between -4 kPa to +4 kPa. Two pressure gauges (3D instruments, DTG-6000) at each of the inlet and outlet terminals of the porous tube provided the internal pressure reading. The pressure difference between the input and the output of the tube was negligible. Dissolved oxygen level on the porous tube surface was monitored using a commercial Clark type oxygen probe (Harvard/Instech, AH-56-5002, diameter 3.2 mm, length 41.3 mm). The permeable hydrophobic membrane and internal electrolyte of the commercial probe were replaced once for every experimentation cycle. The oxygen microsensor array was connected to the instrument using a zero-insertion force connector as shown in the picture in figure 3. Initially the microsensor was placed in a measuring vessel and pre-polarization of the sensor was performed for 15-20 minutes before the actual measurements. Later, the microsensor array was applied on the porous tube and the calibration and measurements were performed at different oxygen saturation\concentration levels of internal solution and different internal pressures. The flexible oxygen microsensor array is enwrapped around the porous tube as in figure 4(a) whereas the 4-point electrodes are placed on the surface along the length of the tube as in figure 4(b). The outer pair of current probes minimizes the influence of contact impedance of the voltage probes during the impedance measurement. All measurements were performed at room temperature (23° C ± 1° C).

3. Instrumentation

A custom set of electrochemical instrumentation has been employed for experiments involving the microsensor. A potentiostat (Gamry Instruments, PC4-FAS1) was used along with a multiplexer (Gamry Instruments, ECM8) to individually address the 4 oxygen microsensors in a strip. A separate source-measure unit (Keithley Instruments, SCS-4200) was used to measure oxygen responses with the commercial probe. To equilibrate the solution to the desired oxygen saturation level, a fixed ratio of oxygen and nitrogen gases were bubbled in the reservoir using two mass flow controllers (MFC) (MKS Instruments, 1159B). The operation of the MFC was controlled using a 4 channel readout power supply (MKS Instruments, 247C). A potentiostat (Gamry Instruments, PC4-750) was used to perform the 4-point impedance measurements. Electrochemical characterization of the microsensor was performed using linear sweep voltammetry (LSV) and chronoamperometric (CA) methods. The LSV was used to determine the cathode oxygen reduction voltage of the working electrode. The CA measurements were made to obtain the oxygen responses with respect to time. The conductivity measurement was performed with a current density of 0.1 $mA/cm^2$ (rms) at the frequency of 1 kHz.

## III. RESULTS AND DISCUSSION

1. Electrochemical characterization in bulk solution

Microsensor characterization was performed in plant nutrient solution (quarter strength Hoagland's solution, pH 5.8–6). LSV measurements were made over a voltage range of 0.0 to -1.0 V at a step decrement of 50 mV/s starting at 0 V. For potentials between 0 to -0.6 V, reaction rates were dependent on both rates of charge transfer of oxygen reduction as well as mass transport of oxygen towards cathode. For potentials between -0.6 to -0.8 V, the limiting current plateau was observed which implies that the reaction rate was determined by only the mass transport. For any lower potential, hydrogen evolution due to water decomposition causes a steep increase in current. So the cathodic potential for oxygen reduction was chosen as -0.7 V vs. Ag/AgCl as it has a minimum reduction of species other than oxygen [16]. Chronoamperometric measurements were performed and the resultant transient responses of the microsensor, for varying oxygen saturation levels (concentrations), are shown in figure 5(a). The response time to achieve steady-state limiting current was about 20 seconds. The corresponding calibration curve is shown in figure 5(b). The sensor response is plotted both in terms of oxygen concentration (μmol/L) as well

as gas phase oxygen saturated in nutrient solution (%). During conversion of values from gas phase oxygen saturated in solution to oxygen concentration, a salinity factor of 2.3 g/L for the Hoagland's solution is taken into consideration. The sensor response is linear and repeatable over the gas phase oxygen saturation range of 0 % (2.2 μmol/L) to 50 % (521.9 μmol/L). This is in agreement with the limiting current theory where the relationship between limiting current magnitude and oxygen concentration is linear [14, 16]. But the linearity is not maintained well over the gas phase 50 % oxygen saturation level (i.e. 521.9 μmol/L $O_2$ concentration). This could be attributed to a possible reduction of oxygen catalytic activity due to increase in the local pH near the working electrode at higher oxygen level [16]. The limiting current in unstirred bulk plant nutrient solution was approximately 50 % lower than stirred solutions as in figure 5(a). The slope of the calibration curve is higher for stirred condition, as in figure 5 (b), showing that the nutrient solution is well replenished and having higher mass transport rate when compared to unstirred condition. Importantly, it is noted that when the sensor is in direct contact with the porous tube the stir sensitivity would be reduced to a great extent or eliminated. Bare sensors exhibited higher currents than sensors with poly-HEMA coating as the mass transport rate was higher without this hydrophilic coating. A small amount of residual current was observed at zero saturation (2.2 μmol/L $O_2$ concentration) level.

2. Oxygen microsensors:

A commercial Clark type dissolved oxygen probe was initially used to serve as a reference for the microsensor results. A 2-point calibration was performed on the porous tube surface at 2.2 μmol/L and 178.1 μmol/L oxygen concentrations that correspond to 0% and 20 % $O_2$ gas bubbled in internal solution at the highest positive pressure (3.0 kPa). All data points in figure 6(a) were based on these calibration points, since the reliable calibration procedure was possible only when the probe was bathed in a sufficient water film in positive pressure. Therefore probe responses at higher positive internal pressures properly reflect the oxygen concentration value of the inner solution. At lower positive pressures less water film will be formed and subsequently the probe will be only partially in contact with the internal solution and partially exposed to the gaseous oxygen in air (21 %). Thus the responses start to show reduced sensitivity to dissolved oxygen in the water film. At zero pressure and negative internal pressures, the probe response converges to air saturation values. This is because there will be little water film on the tube surface and the sensor response is mainly affected by the gaseous oxygen available from the environment owing to negligible stirring sensitivity of the commercial probe. But the extremely little presence of

water film at zero or negative pressures leads to a deviation of the probe response away from the air saturation value. Figure 6(b) shows the linear calibration response of the probe depending on the internal pressure. When little water film is formed on the tube surface (i.e. negative or zero pressure), the calibration curve exhibits almost zero slope. As the film thickness is increased, the slope of the calibration curve gradually increases as the internal solution comes into contact with the probe surface. The maximum slope is observed when enough water film is formed on the tube at high positive pressures.

The microsensor characterization was performed in a similar manner as the commercial probe. It was first subjected to prepolarization (preconditioning) for 15-20 minutes before the actual measurement and then subjected to chronoamperometric tests. Each sensor in a strip was separately multiplexed by the pulsatile cathodic oxygen reduction voltage. The calibration was performed by bubbling gaseous oxygen at 0 % and 20 % $O_2$ in nutrient solution (i.e. 2.2 μmol/L and 178.1 μmol/L oxygen concentrations respectively) on the tube surface at the highest pressure (3.0 kPa). The microsensor response, shown in figure 7(a), was similar to the commercial probe response at positive pressure. The response curve value, for a fixed oxygen saturation level, increases as water film thickness on the surface increases. The microsensor reflects oxygen levels properly with enough water film on the tube surface. It should be noted that, however, the sensitivity almost saturated in a less positive pressure (1.5 kPa). This fact implies that the thin film microsensor is useful for oxygen detection with very small sample amount or in microscale local environment. But the responses at negative pressures were scattered around the 2.2 μmol/L oxygen concentration value and measurements were not reliable due to surface dryness and absence of sensor hydrophobic membrane of the Clark type sensor. There can be another reason for the decreasing sensitivity at lower pressures. As shown in figure 5(b), the microsensors showed higher sensitivity towards stirring than commercial probes due to the absence of a hydrophobic membrane. Since the calibration was performed once at highest positive pressure only, the probe response deviates from the actual values as the pressure decreases due to varying stirring conditions. Therefore, the deviation along with scattering is significant at zero and negative pressures due to both stirring effect and insufficient water film. But at positive pressures, problems arising due to insufficient water film are not much significant compared to stirring effect. The calibration curve in figure 7(b) shows that the slope is positive whenever there is a presence of water film on the porous tube surface and increases with increase in the liquid film thickness for a fixed oxygen concentration level. Further increase of the film thickness, by increasing the internal pressure of the porous tube, will not yield any substantial increase in the slope of the calibration curve.

3. Conductivity microprobe:

When the surface is dry, impedance between the probes is very high as there is no suitable conducting medium (plant nutrient solution). Gradual decrease of impedance in negative pressure region as shown in figure 8 implies that the water content within the porous tube media is increasing due to the decreasing suction capability. This result suggests a possibility of using the conductivity probe in measuring the moisture contents in unsaturated particulate plant growth media in combination with pulse moisture sensor [12]. A steep transition towards lower impedance value at the moderate negative pressure is considered to be due to the capillary effect to contain the solution in the porous tube media. Once the pore portion in the tube is saturated with solution solely by the capillary force in the zero pressure, the impedance showed almost the least value. This implies that the contribution of surface water film to conductivity is negligible compared to that of saturated porus media. For positive pressures, there is no clear differentiation between the different levels of liquid film thickness on the wet tube surface. The results for both 2-probe and 4-probe impedance measurements were compared and it was found that 4-probe demonstrates lower average impedance values along with higher percentage of difference between wet and dry surface values by minimizing the effect of contact impedance between the electrode and the solution.

## IV. CONCLUSION

First, a microfabricated dissolved oxygen sensor array is presented. For space missions, it is desirable to have dissolved oxygen sensors that can measure oxygen concentrations in a way that is standardized and prevents artifacts associated with the spaceflight environment. While this sensor does not directly measure oxygen bioavailability in root zone, it does directly measure oxygen concentrations in the root zone, without having water content or root growth in the immediate sensor zone to impact these measurements. The response of the oxygen microsensor is comparable with the performance of the commercial Clark type probe on the tube surface with regard to oxygen concentration measurements. The microsensors work effectively in the presence of water film. The results suggest that the microsensors are capable of determining oxygen saturation on the porous tube surface, where the stir-sensitivity of sensor would be minimized, yet would insure maximum sensitivity. Additionally, a 4-point microprobe for wetness detection in the porous tube system is discussed. The 4-point impedance probes clearly differentiate between wet and dry surfaces. Results suggest that the microprobes are capable of determining porous

media wetness on the porous tube surface. These microsensors and microprobes could be employed for plant root zone monitoring in varied fluid delivery systems that are being developed especially the porous tube nutrient delivery system and the particulate based system. Further sensor developments are focused on achieving enhancement of integrated microsensors along with on-chip structural integration in monitoring systems.

**ACKNOWLEDGEMENTS**

This research was supported by a grant from the NASA Office of Biological and Physical Research (01-OBPR-01).

**REFERENCES**

1. Monje,O.; Stutte,G.W.; Goins, G.D.; Porterfield, D.M.; Bingham, G.E., Farming in Space: Environmental and Biophysical Concerns. Advanced Space Research Vol. 31: 151-167; 2003.
2. Dreschel, T.W.; Carlson, C.W.; Wells, H.W.; Anderson, K.F., Physical testing for the microgravity plant nutrient experiment. Paper No 93-4007, American Society of Agriculture Engineers, Spokane, Washington; 1993.
3. Porterfield, D. Marshall, The biophysical limitations in physiological transport and exchange in plants grown in microgravity. Journal of Plant Growth Regulation. 21: 177-190; 2002.
4. Liao, J., Liu, G., Monje, O., Stutte, G.W., Porterfield, D.M., Induction of hypoxic root metabolism results from physical limitations in O2 bio-availability in microgravity. Adv. Space Res. , 2004.(In press)
5. Levine, Howard; Piastuch, W.C; Dreschel, T.W., Development of a microgravity rated hydroponic plant culture apparatus. Proceedings of the 36th Space Congress: 295-302; 1999.
6. Porterfield, D.M.; Dreschel, T.W.; Musgrave, Mary E., A ground based comparison of nutrient delivery technologies developed for growing plants is spaceflight environment. HortTechnology 10: 179-185; 2000.
7. Dreschel, T.W.; Brown, C.S.; Piastuch, W.C.; Knott, W.M., Porous tube plant nutrient delivery system development: A device for nutrient delivery in microgravity. Advanced Space Research Vol. 14: (11)47-(11)51; 1994.

8. Burtness, Kevin; Norwod, Kelly; Murdoch, Trevor; Levine, Howard, Development of a porous tube based plant growth apparatus. Paper No. 2002-01-2389, 32nd International Conference on Environmental Systems, San Antonio TX; 2002.
9. Dreschel, T.W.; Brown, C.S.; Piastuch, W.C.; Hinkle, C.R., A summary of porous tube plant nutrient delivery system investigations from 1985 to 1991. NASA Technical Memorandum 107546, Jan 1992.
10. Tsao, David T.; Okos, Martin R.; Sager, John C., Controlling the water availability from a ceramic tube system subjected to non-standard gravities. SAE Technical paper series #961505, Monterey CA; 1996.
11. Dreschel, T.W.; Sager, John C., Control of water and nutrients using a porous tube: A method for growing plants in space. HortScience, Vol. 24: 944-947; 1989.
12. Clark, G.J.; Neville, Jr.; Dreschel, T.W., A root moisture sensor for plants in microgravity. Advanced Space Research, Vol. 14: (11)213-(11)216; 1994.
13. Schneiderman, Gary; Goldstick, Thomas K., Oxygen electrode design criteria and performance characteristics: recessed cathode. Journal of applied physiology, Vol. 45: (1)145-(1)154; 1978.
14. Lambrechts, M.; Sansen, W., Biosensors: microelectrochemical devices, IOP Publishing, 1992.
15. Buck, R.P.; Lindner, V.V.Cosofret; Ufer, S.; Madaras, M.B.; Johnson, T.A.; Ash, R.B.; Neuman, M.R., Microfabrication technology of flexible membrane-based sensors for in-vivo applications. Electroanalysis, Vol. 7: 846-851; 1995.
16. Linek, V.; Vacek, V.; Sinkule, J.; Benes, P., Measurement of Oxygen by Membrane-covered Probes. Ellis Horwood; 1988.

**FIGURE CAPTIONS**

**Figure 1.** Porous tube nutrient delivery system in microgravity. The plants are grown on the porous tube surface and the nutrient solution is delivered to the root zone through the pores in the tube by capillary force. The system efficiently ensures no free liquid escapes, provides a uniform distribution of water and nutrients within the root zone and maintains adequate oxygen levels at root zone. The porous tube provides efficient capillary interface between plant nutrient solution and plant roots.

**Figure 2. (a)** Cross-section of 3-electrode amperometric oxygen microsensor on flexible polyimide (Kapton®) substrate (1. substrate cleaning, 2. metallization of Pt/Cr and photolithography, 3. polyimide photolithography). The 3-electrode cell minimizes the ohmic voltage drop through the electrolyte between the anode and cathode and prevents the consumption of reference electrode material. Cell design comprises of platinum concentric electrodes to ensure symmetric diffusional mass transport of electrochemical species in all radial directions. The center electrode serves as the reference electrode (RE) (exposed diameter of 100 μm). This is later electroplated with Ag/AgCl on the reference electrode The next concentric circle is used as the working electrode (WE). The spacing between two successive concentric electrodes is 100 μm., **(b)** Photograph of the oxygen microsensor strip including an array of 4 sensors. The dissolved oxygen sensor strip made of flexible polyimide substrate consists of 4 microsensors. The strip is 58 mm long and 6 mm wide. This length enables the placement of sensors at equidistance of 10 mm when they are enwrapped on the porous tube surface.

**Figure 3.** A schematic of the plant nutrient delivery system and the associated instrumentation. The system includes a 1 liter liquid reservoir to store the plant nutrient solution. A gear pump draws out the solution from the reservoir and into the alumina porous tube (Refractron, porosity 0.5 μm, OD 13 mm, ID 8 mm, length 100 mm) at a constant flow rate of 15 ml/min. The internal pressure of the tube can be either positive or negative depending on the polarity of the pump direction. A valve on each side of the tube controls the internal pressure between -4 kPa to +4 kPa. Two pressure gauges (3D instruments, DTG-6000) at each of the inlet and outlet terminals of the porous tube provide the internal pressure reading. A closer look at the oxygen microsensor strip enwrapped around the porous tube and attached to the connector.

**Figure 4. (a)** Cross-section of the porous tube with the oxygen microsensor strip (with 4 microsensors) enwrapping with the sensor in contact with the tube surface. The 4 sensors are placed equidistant from each other on the surface., **(b)** 4-probe conductivity microprobe placed along the surface with probes 1 and 4 as current probes and probes 2 and 3 as voltage probes, respectively. Each identical electrode has a diameter 500 μm. The spacing between the current probes and the voltage probes are 80 mm and 76 mm, respectively. The outer pair of current probes minimizes the influence of contact impedance of the voltage probes during the impedance measurement. All measurements were performed at room temperature (23° C ± 1° C).

**Figure 5. (a)** Typical transient chronoamperometry responses of oxygen microsensor for an applied cathodic potential of -0.7 V vs. Ag/AgCl at different oxygen concentration levels (with their corresponding gas phase oxygen saturation values) in plant nutrient solution (quarter strength Hoagland's solution, pH 6.0, room temperature) for stirred and unstirred conditions. The sensor response is linear and repeatable over the gas phase oxygen saturation range of 0 % to 50 % $O_2$ (i.e. 2.2 μmol/L to 521.9 μmol/L $O_2$ concentration). **(b)** Calibration curve from the limiting current values measured at time = 30 seconds in the chronoamperometry test. The limiting current in unstirred bulk plant nutrient solution shows approximately 40 % lower values than stirred solutions showcasing the microsensor's stir sensitivity. The slope of the calibration curve is higher for stirred condition when compared to unstirred condition.

**Figure 6. (a)** Surface dissolved oxygen measurement with a commercial Clark-type mini-probe with respect to different internal pressures of nutrient solution within the porous tube with different oxygen concentration levels (with the corresponding gas phase oxygen saturation in solution values) of inner nutrient solution. Probe responses at higher positive internal pressures properly reflect the oxygen value of the inner solution. Thicker water films are not easily affected by gaseous oxygen in air (21%). As water film thickness decreases, probe responses start converging to air saturation values., **(b)** Replot of (a) with respect to different oxygen concentration levels to show the sensitivity depending on the internal pressure. With little water film formed on the tube surface (i.e. negative or zero pressure), the calibration curve exhibits almost zero slope. As the film thickness increases, the slope of the calibration curve gradually increases as the internal solution comes into contact with the probe surface.

**Figure 7. (a)** Surface dissolved oxygen measurement with a microsensor array with respect to different internal pressures of nutrient solution within the porous tube with different oxygen concentration levels of inner nutrient. The response curve value, for a fixed oxygen concentration level, increases as water film thickness on the surface increases. The microsensor reflects oxygen levels properly with enough water film on the tube surface. The responses at negative pressures are scattered around the lowest oxygen concentration value and measurements are not reliable due to surface dryness and absence of sensor hydrophobic membrane., **(b)** Replot of (a) with respect to oxygen saturation\concentration levels to show the sensitivity depending on the internal pressure. The calibration

curve shows that the slope is positive whenever there is a presence of water film on the porous tube surface and increases with increase in the liquid film thickness for a fixed oxygen concentration.

**Figure 8.** Surface wetness measurement with a 4-point microprobe showing a gradual decrease of surface impedance at the transition from negative to positive pressure. Dry surface shows higher impedance between the probes as there is no suitable conducting medium. Gradual decrease of impedance in negative pressure region implies that the water content within the porous tube media is increasing due to the decreasing suction capability. Steep transition towards lower impedance value at the moderate negative pressure is due to the capillary effect to contain the solution in the porous tube media. Impedance is least when the pore portion in the tube is saturated with solution.

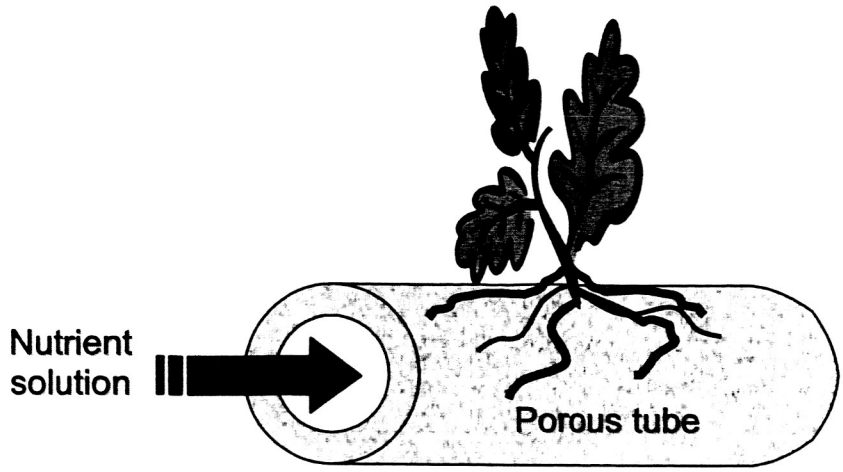


**Figure 1**

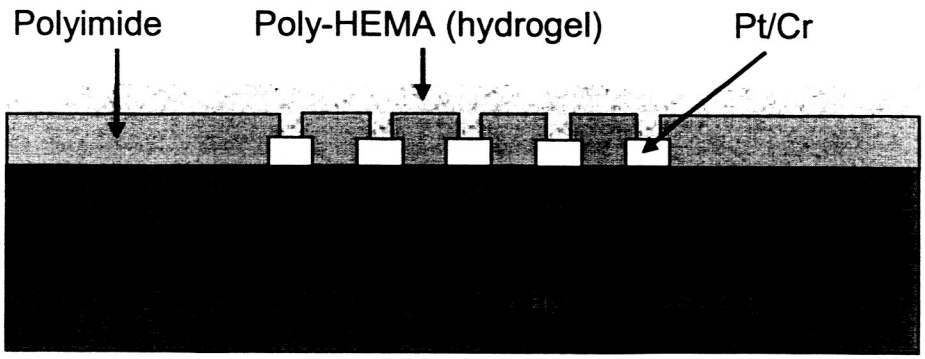


**(a)**

**(b)**

**Figure 2**

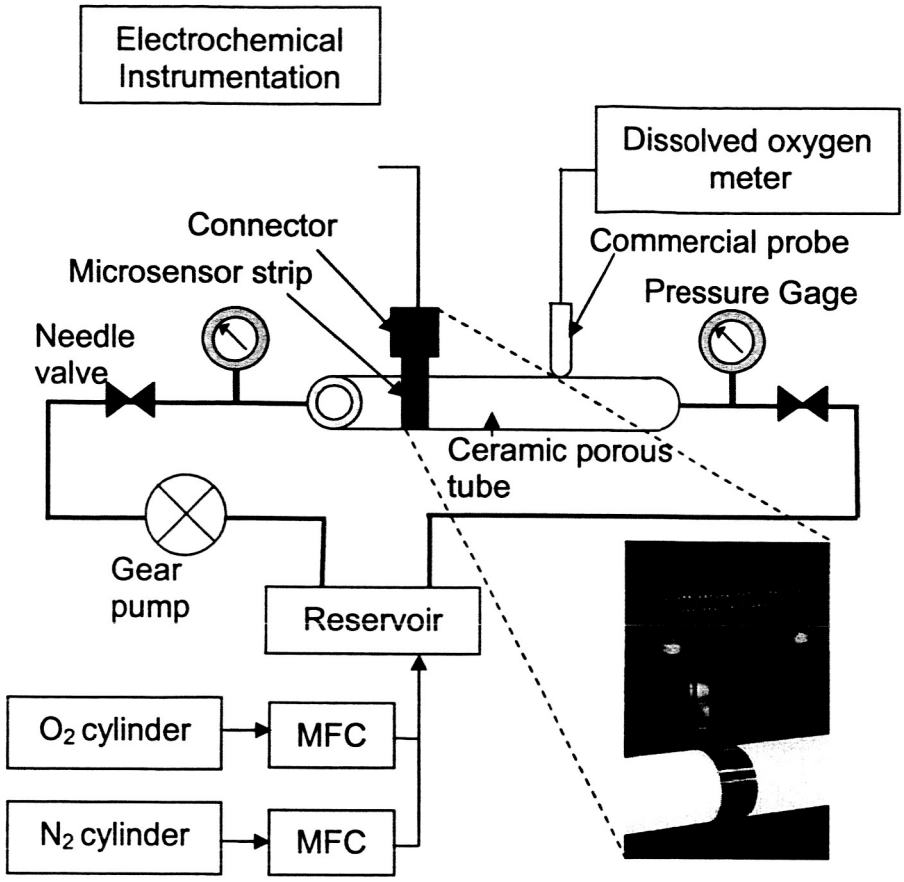
Electrochemical Instrumentation
Dissolved oxygen meter
Connector
Microsensor strip
Commercial probe
Pressure Gage
Needle valve
Ceramic porous tube
Gear pump
Reservoir
$O_2$ cylinder
MFC
$N_2$ cylinder
MFC

**Figure 3**

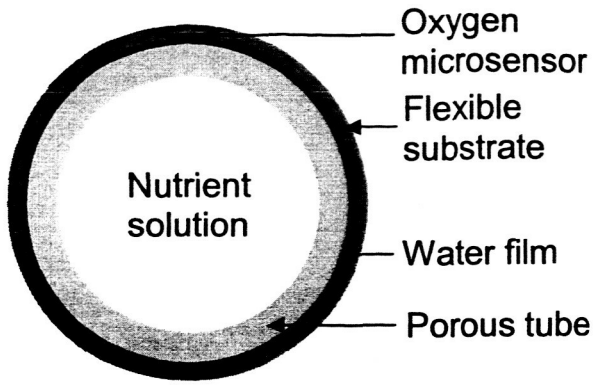


**Transversal cross-section**

**(a)**

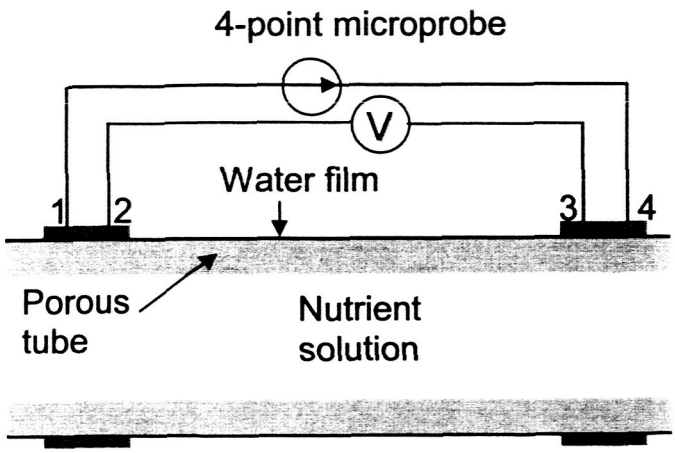


**Longitudinal cross section**

**(b)**

**Figure 4**

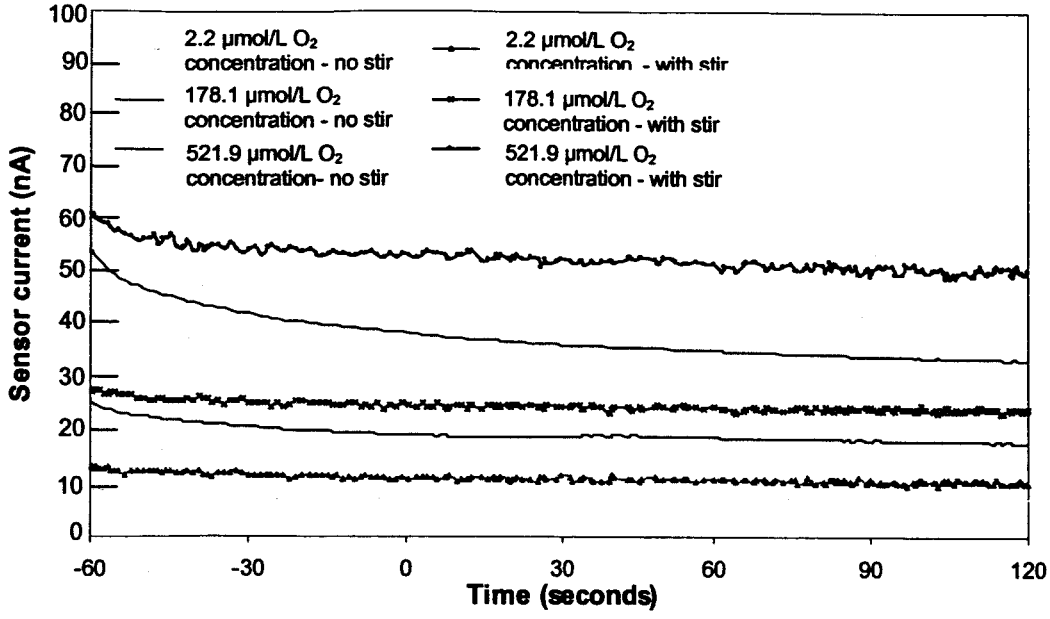


(a)

**Figure 5 (a)**

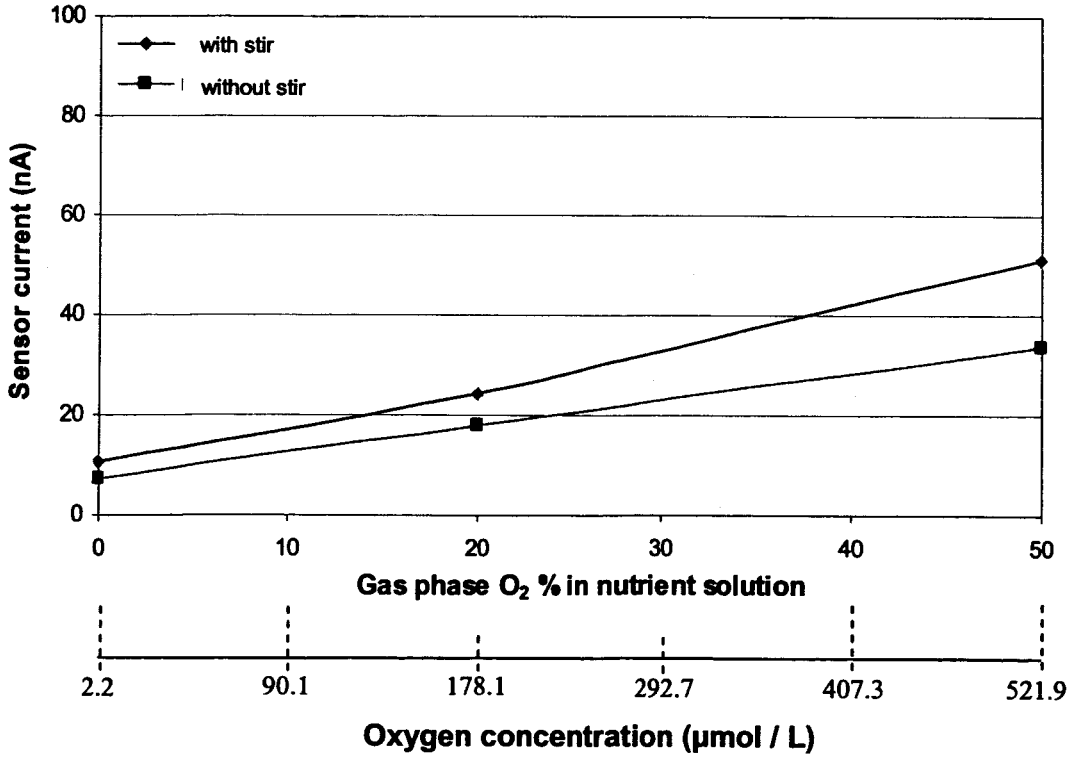


(b)

**Figure 5 (b)**

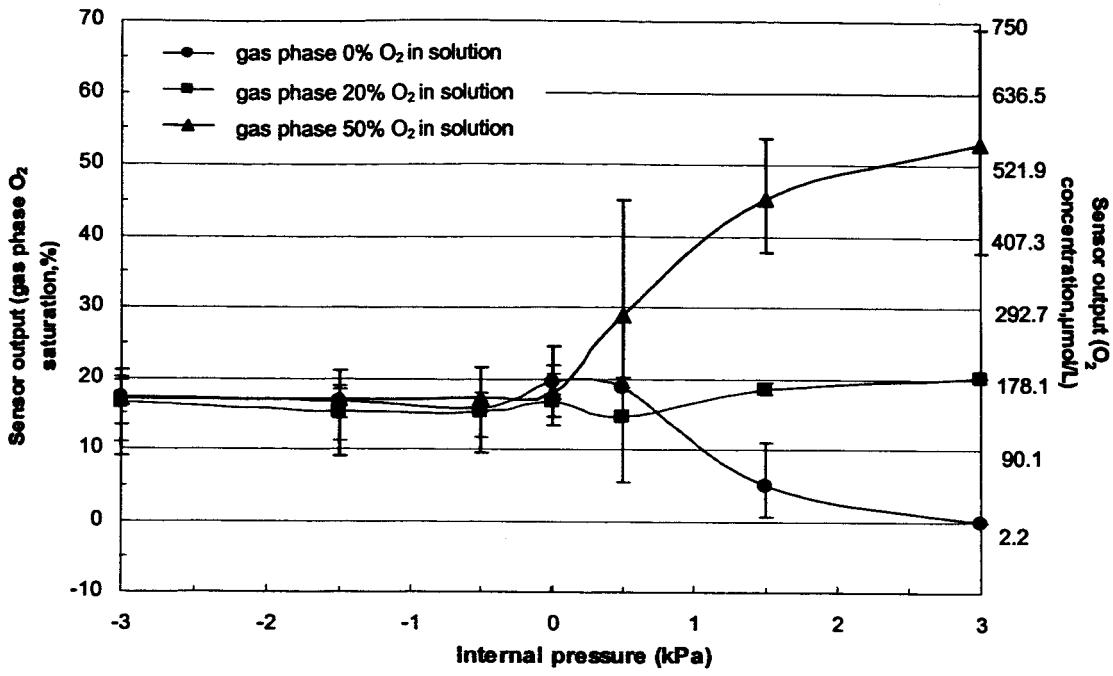


(a)

**Figure 6 (a)**

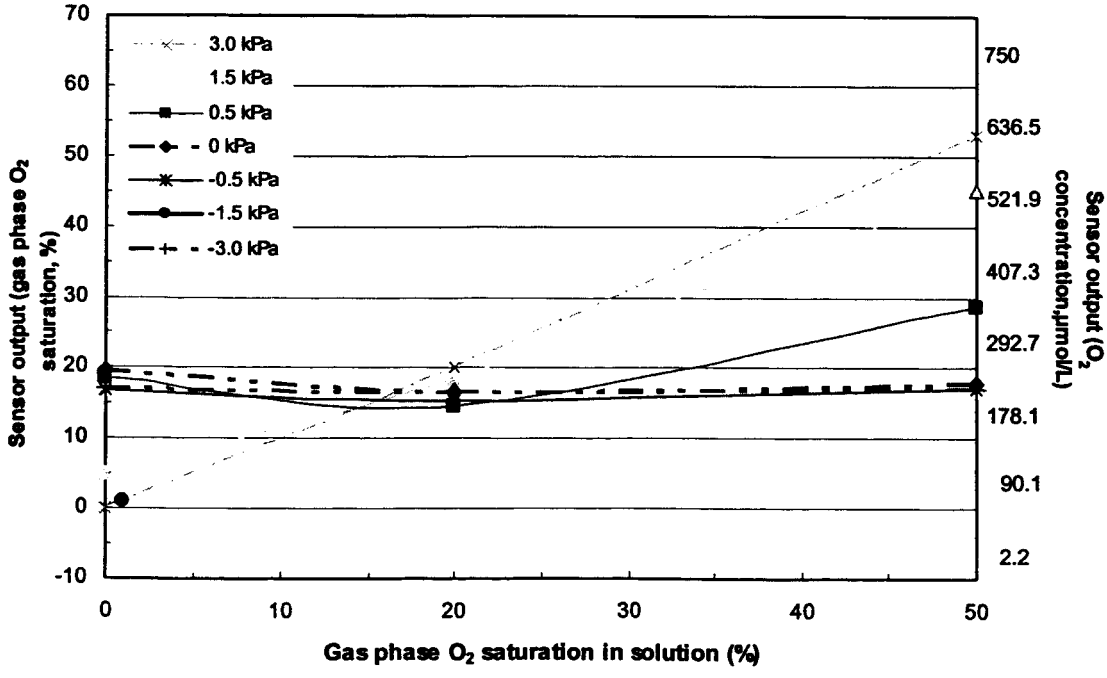


(b)

**Figure 6 (b)**

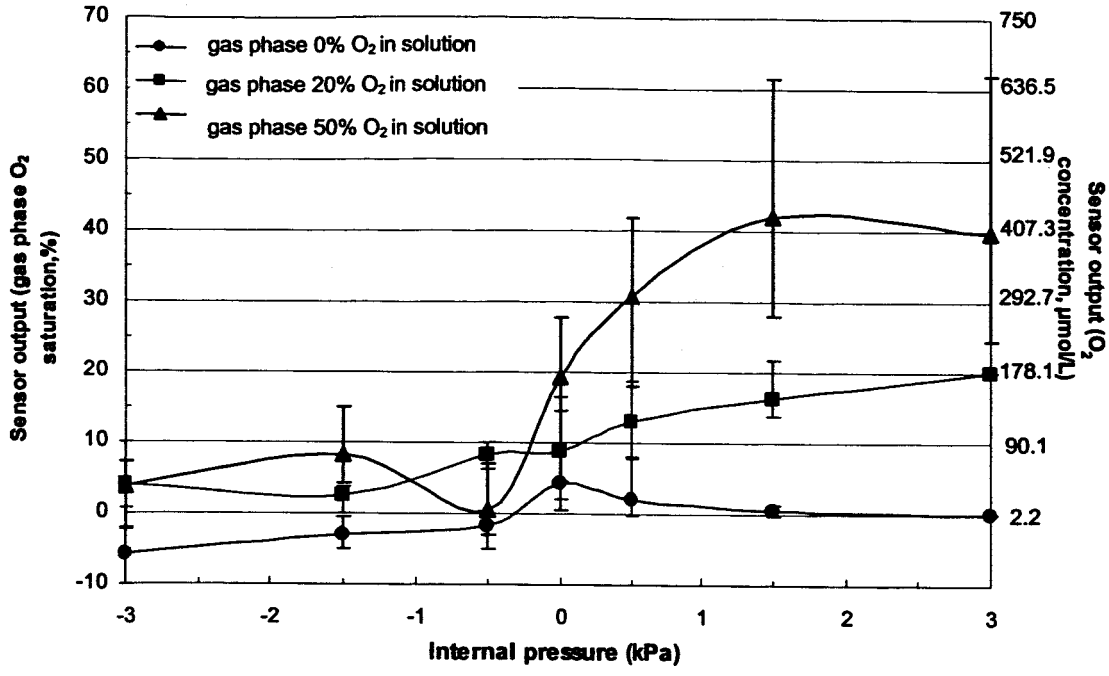


(a)

**Figure 7 (a)**

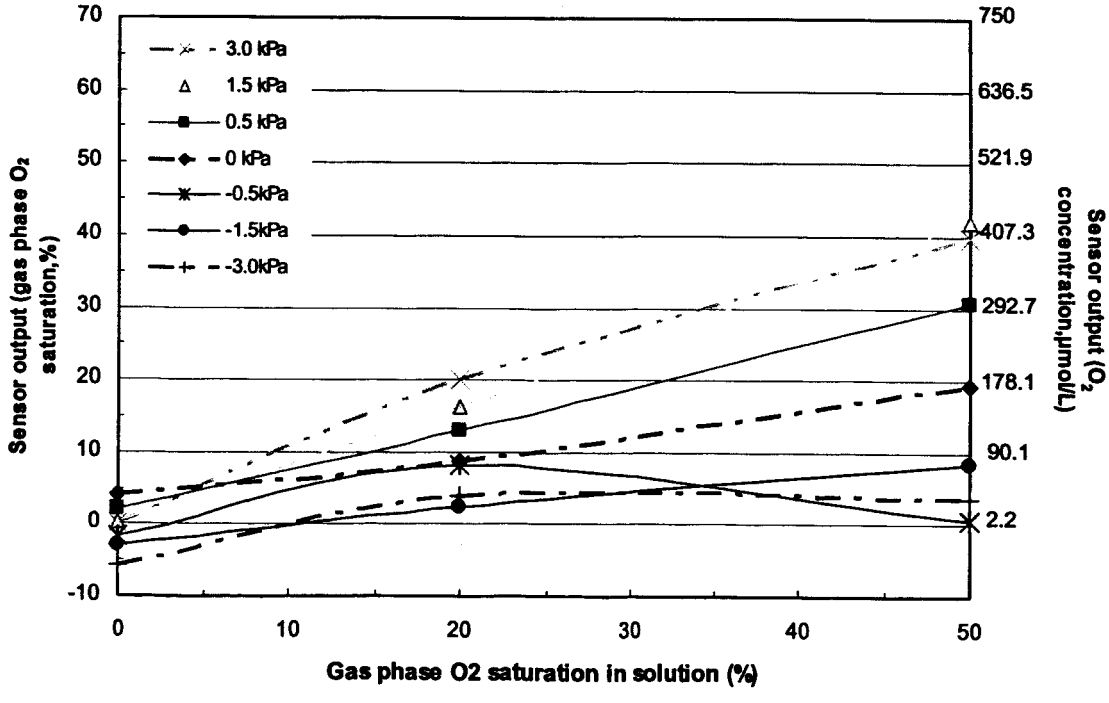


(b)

**Figure 7 (b)**

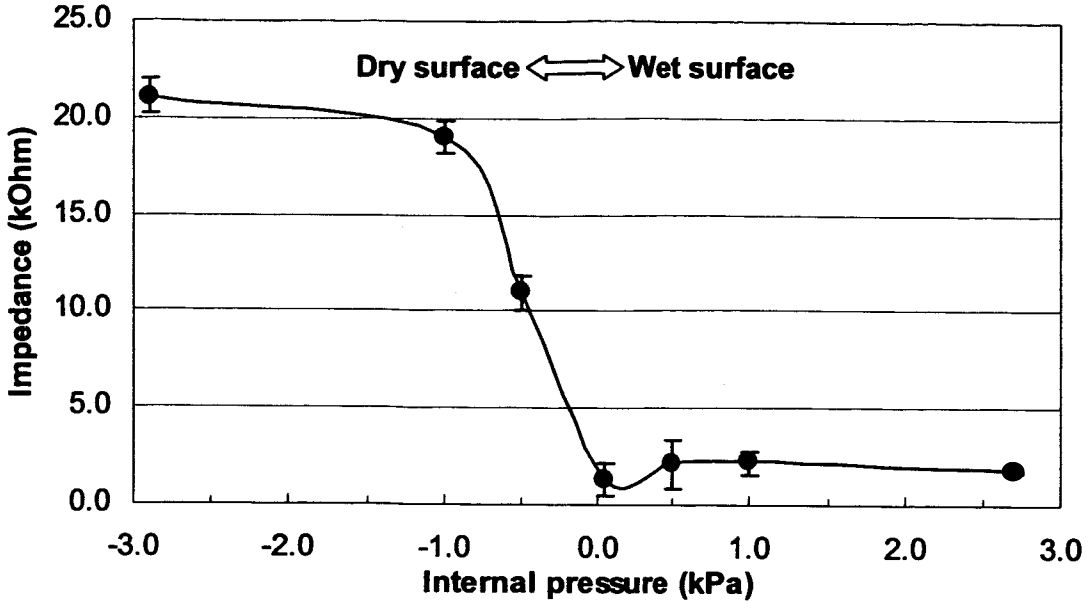
25.0
20.0
15.0
10.0
5.0
0.0
Impedance (kOhm)
Dry surface ⟺ Wet surface
-3.0
-2.0
-1.0
0.0
1.0
2.0
3.0
Internal pressure (kPa)

**Figure 8**

## Appendix 3 (abstract presented at IEEE Sensors Conference 2004)

Topic: 3

# Electrochemical and hydrodynamic Interferences on the Performances of an Oxygen Microsensor with Built-in Electrochemical Microactuator*

Chang-Soo Kim [1,2], Chae-Hyang Lee [1]

(1) Dept. of Elect. & Comp. Eng., Univ. of Missouri-Rolla, Rolla, MO, ckim@umr.edu,
(2) Dept. of Biological Sciences, Univ. of Missouri-Rolla, Rolla, MO.

**Summary**

A concept of novel electrochemical *in situ* self-calibration technique for an oxygen microsensor has been proposed to devise a convenient calibration method without an externally coupled apparatus[1]. Systematic investigations on the influences of various electrochemical (pH) and hydrodynamic (solution stirring) conditions on the proposed microsensor performances are presented. The results suggest that (1) the calibrating microenvironments can be manipulated with carefully engineered sensor designs and optimized generating signals, and (2) the external oxygen permeable membrane is needed to minimize the electrochemical and hydrodynamic interferences.

**Motivation**

The importance of continuous chemical monitoring cannot be overemphasized to realize autonomous and unattended instrumentation. A dependable self-calibration method is required to achieve reliable biochemical sensor system[2]. The proposed method addresses a novel *in situ* self-calibrating oxygen microsensor based on water electrolysis by using an integrated electrochemical actuator (generating electrode, GE)[1] (Fig. 1). This technique is expected to enable periodic *in situ* self-calibration and self-diagnosis of microsensor during real-time oxygen monitoring and will lead to intelligent devices with on-board, self-calibration features.

**Results**

We designed and fabricated polarographic oxygen microsensors on a flexible Kapton® (polyimide) substrate. A potentiostat and a constant current source were used to bias the microsensor (three-electrode cell) and to provide generating signal to GE, respectively (Fig. 2). The actuation procedure involved an oxygen-generating phase during sensor operation. The chronoamperomtric responses increased during the oxygen-rich phase, and then gradually returning to the original level of air-saturated solution (Fig. 3a). In a strong pH buffer solution the sensor showed much diminished oxygen responses during this phase (Fig. 3b). In both cases the responses exceeded those in the oxygen-saturated solution. These imply the effect of bulk pH on the catalytic activity of cathodic oxygen reduction due to the local pH change accompanied by water electrolysis. Stirring of the solution reduced the oxygen responses by disturbing the local microenvironment as expected (Fig. 3c). The responses during the oxygen-depletion phase approached to that in the nitrogen-saturated (oxygen-depleted) solution (Fig. 3d).

1. C. S. Kim, J. O. Fiering, C. W. Scarantino, H. T. Ngin, "A novel in situ self-calibration method for an oxygen microsensors," World Congress on medical Physics and Biomedical Engineering, Chicago, 2000.
2. P. Yager, "Biomedical sensors and biosensors," in B. D. Ratner, *et al.* (eds), Biomaterials Sciences, Academic Press, 1996.

* Acknowledgement: this research was funded in part by a grant from the OBPR, NASA (01-OBPR-01).

Figure 1. Concept of an electrochemical *in situ* self-calibration of oxygen microsensor. Microsensor can be confined in a controlled microenvironment during the oxygen-saturation and oxygen-depletion phases depending on the polarity of generating electrode (GE).

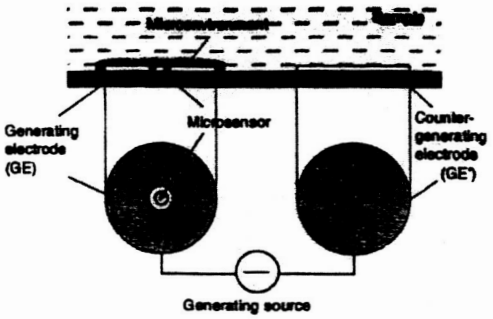


Figure 2. Measurement scheme for chronoamperometric responses. A potentiostat is employed for the 3-electrode oxygen microsensor, a constant current source for generating microenvironments, respectively.

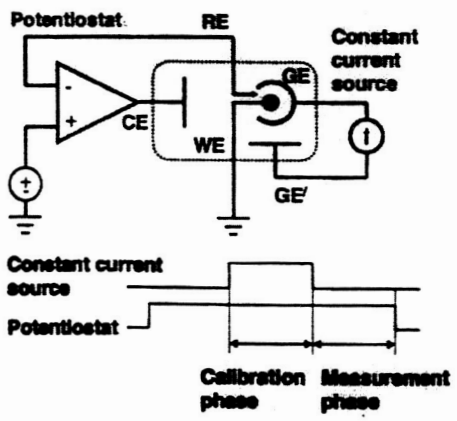


Figure 3. Changes in oxygen microenvironment around the microsensor manipulated by the surrounding generating electrode; chronoamperometric responses during the oxygen-generating phase with various generating current signals compared with that in oxygen-saturated solution (top curve) (a) in an air-saturated plant nutrient solution (quarter strength Hoagland solution), (b) in an air-saturated phosphate buffer solution, (c) in an air-saturated vigorously-stirred phosphate buffer solution; chronoamperometric responses during the oxygen-depleting phase with various generating current signals compared with that in nitrogen-saturated solution (bottom curve) (d) in an air-saturated phosphate buffer solution.

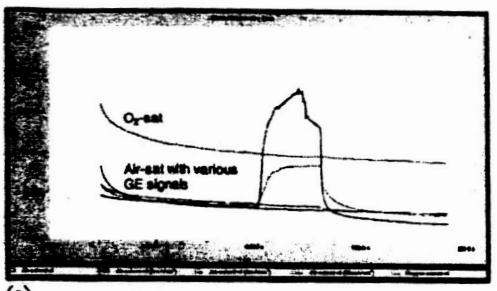


(a)

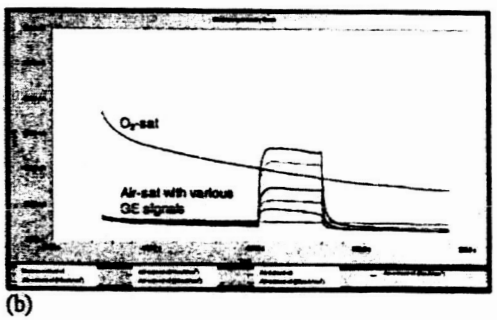


(b)

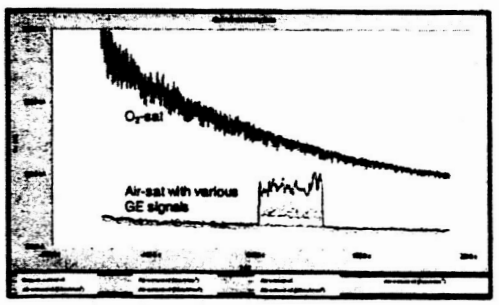


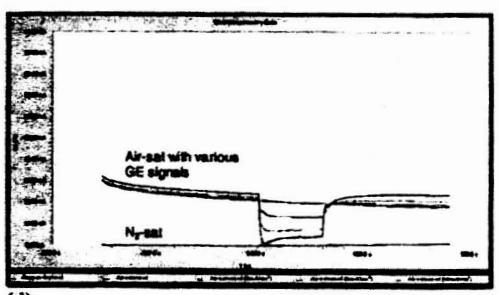


(d)

Slide 1

## Electrochemical and Hydrodynamic Interferences on the performance of an Dissolved Oxygen Microsensor with Built-in Electrochemical Actuator

Chang-Soo Kim[1,2]
Chae-Hyang Lee[1]

(1) Dept. of Electrical & Computer Engineering, University of Missouri-Rolla
(2) Dept. of Biological Sciences, University of Missouri-Rolla



Slide 2

## Built-in, on-chip intelligence of biochemical microsensor

- Intelligent microsensor system; unattended, autonomous, self-adaptive, self-regulatory.
- Functional integration as well as structural integration.
- On-chip integration of "biochemical actuation" system to establish dynamic microenvironments.



Slide 3

## Necessity of "*In situ* self-diagnosis and/or self-calibration"

- Periodic correction of slope/ baseline drift, diagnosis of functionality.
- Little *in situ* self-diagnosis and/or self-calibration feature in commercially available sensors.
- One of key obstacles for realization of reliable biochemical sensor for continuous use.

Slide 4

## Dissolved oxygen microsensor with in situ self-diagnosis capability

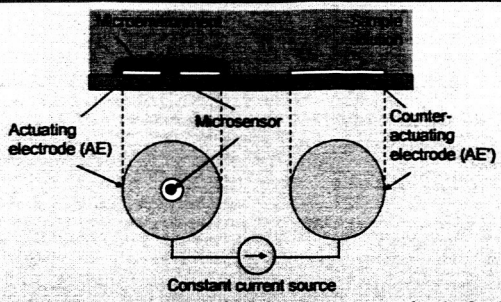


- Microenvironments established by water electrolysis.
- $O_2$-rich or $O_2$-depleted phases according to anodic or cathodic behavior of actuating electrode (AE).



Slide 5

## Microfabrication of 3-electrode amperometric microsensor

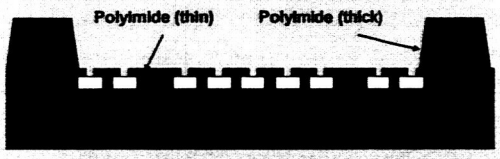


- Substrate: Kapton (polyimide)
- Metal deposition (Pt)
- Photoresist lithography
- Metal etching
- Polyimide lithography (thin)
- Polyimide lithography (thick)



Slide 6

## Instrumentation and operation modes

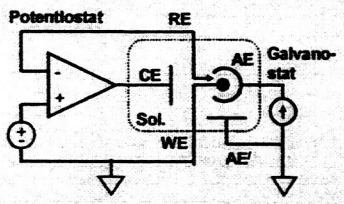


- Electrically-floated operation of a potentiostat and a galvanostat.

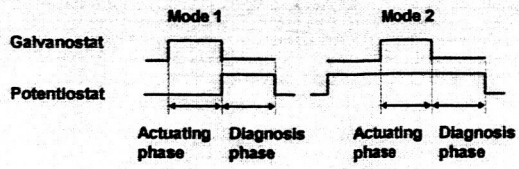

Slide 7

## Transient sensor responses after $O_2$-generating actuation phases of various duration (mode1)

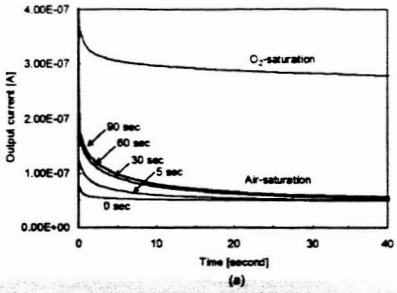


(a)

- Initial values approaching that of $O_2$-saturation; $O_2$-rich microenvironments (actuating current density: 5mA/cm$^2$).
- Convergence to background response; being equilibrated with surrounding medium shortly.



Slide 8

## Transient sensor responses after $O_2$-depleting actuation phases of various duration (mode1)

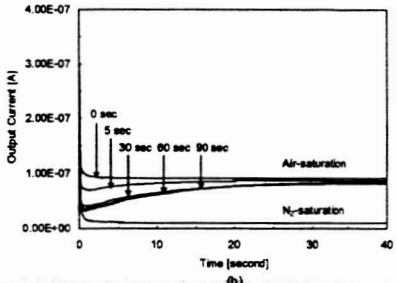


(b)

- Initial valued approaching that of $N_2$-saturation; $O_2$-depleted microenvironments (actuating current density: 5mA/cm$^2$).
- Convergence to background response; being equilibrated with surrounding medium shortly.



Slide 9

## Steady-state responses during $O_2$-generating actuation phases of various current density (mode 2)

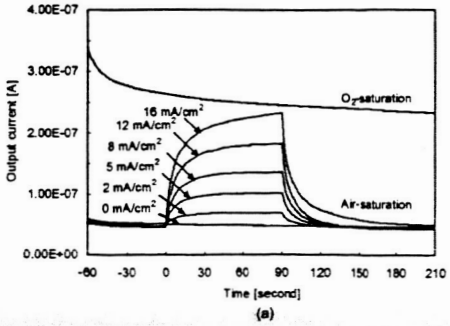


(a)

- Approaching to $O_2$-saturation value with increasing actuation current density.

Slide 10

## Influence of vigorous stirring on the microenvironment (mode 2)

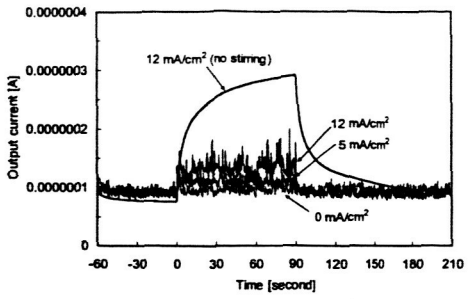


- Diminished responses due to stirring effect; mostly chemical responses with negligible electrical interference (if any).



Slide 11

## Steady-state responses during $O_2$-depleting actuation phases of various current density (mode 2)

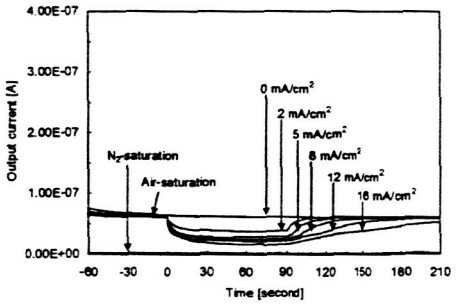


(a)

- Approaching $N_2$-saturation ($O_2$-depletion) value with increasing actuation current density.



Slide 12

## What is going on in the microenvironment?

- Super-saturation; excessive solubility of electrochemically generated dissolved gas.
- Dependence of sensitivity on pH; coefficient = 2 (high pH) ~ 4 (low pH).
- Concentration-driven convection of oxygen; from AE to WE.
- "Feedback" of $H_2O_2$; from WE to AE.
- Local temperature elevation; actuation current density.

Slide 13

## Conclusion and future works

- Controlled oxygen microenvironments with an integrated actuator to provide an on-chip intelligence.
- Need of an external membrane to minimize the electrochemical/hydrodynamic interferences.
- Microfluidic structures for further manipulations to achieve *in situ* self-calibration.
- Applicable to integrated optical sensing platform.

Acknowledgement: NASA grant# 01-OBPR-01

# Appendix 4 (abstract presented at Habitation 2004)



*Abstract MC23*

**An Approach to Model-Based Diagnosis of ALS Subsystems**

Eric Manders
*Research Associate, EECS and ISIS, Vanderbilt University*

Jian Wu
*Graduate Research Assistant, EECS and ISIS, Vanderbilt University*

Jyoti Gandhe
*Graduate Research Assistant, EECS and ISIS, Vanderbilt University*

Surita Gupta
*Graduate Research Assistant, EECS and ISIS, Vanderbilt University*

Gautam Biswas
*Professor, Electrical and Computer Engineering Department, Vanderbilt University*

*Correspondence:* Gautam Biswas, Professor, Electrical and Computer Engineering Department, Vanderbilt University, Box 1829, Station B, Nashville, TN 37235, USA. Phone: 615-343-6204; E-mail: biswas@vuse.vanderbilt.edu

We describe a novel approach for model-based fault detection and isolation of abrupt faults in components of hybrid dynamic systems. Components appear as generic physical parameters in the bond graph model of the system, and parameter changes directly affect system dynamics. Abrupt faults correspond to changes that occur at time scales much faster than the nominal dynamics of the system. We model abrupt faults as discrete and persistent changes in values of component parameters. An abrupt fault in a component parameter results in transients in the system variables. Typically, the transient behavior vanishes after an interval, and for certain faults no evidence of the fault is observable in the measurements after some time. Our approach, named TRANSCEND, is based on the analysis of the fault transient. A novel scheme that uses qualitative analysis of the transient immediately after the onset of the fault with a hypothesize-and-test is employed. To achieve robustness against model uncertainty and noisy measurement data, we combine this qualitative fault isolation scheme with statistical detection and estimation techniques. This solution realizes a signal-to-symbol transformation component that is tailored to the detection of fault transients, and provides robust extraction of features that describe the transient dynamics. We base our solution on a nonparametric signal model, the Discrete Wavelet Transform (DWT) representation of the transient signal, with a decision function that is computed in the transform domain. Symbol generation for fault isolation is aligned with the estimated time point. Symbol generation algorithms are based on linear estimators for the magnitude and derivatives of the signal. The scheme is applied to subsystems of the NASA Advanced Life Support (ALS) system, in particular to components in the Water Recovery System (WRS). We have developed Simulink and bond graph models of the WRS and tuned the nominal parameters of the system using test data provided to us by NASA JSC. We have run simulation studies where we introduce a number of faults in component parameters, and evaluate the fault isolation performance in terms of accuracy and precision. By tuning the symbol generation component to have a near zero error rate in computing the magnitude and derivative symbols, we ensure that fault isolation is always accurate, that is the final hypothesis set always contains the actual fault candidate. Moreover, we demonstrate that fault isolation precision improves with increasing fault size, that is, the final hypothesis set becomes smaller.

Key words: Monitoring; Fault detection; Fault isolation; Dynamic systems; Water recovery system

*Abstract MC25*

**Flexible Microsensor Array for the Monitoring and Control of Plant Growth Environment**

Chang-Soo Kim, Ph.D.
*Assistant Professor, Electrical & Computer Engineering/ Biological Sciences, University of Missouri-Rolla*

D. Marshall Porterfield, Ph.D.
*Assistant Professor, Biological Sciences/Elect & Comp Eng, University of Missouri-Rolla*

H. Troy Nagle, Ph.D., M.D., P.E.
*Professor, Electrical & Computer Engineering, North Carolina State University*

Dr. Christopher Brown
*Director of Space Programs, Kenan Institute for Engineering, Technology & Science, and Department of Botany, North Carolina State University*

*Correspondence:* Chang-Soo Kim, Ph.D., Assistant Professor, Electrical & Computer Engineering/Biological Sciences, University of Missouri-Rolla, 1870 Miner Circle, Rolla, MO 65409, USA. Phone: 573-341-4529; Fax: 573-341-4532; E-mail: ckim@umr.edu

Testing for plant experiments in space has begun to explore active nutrient delivery concepts in which water and nutrients are replenished on a continuous basis for long-term growth. The goal of this study is to develop a novel

microsensor array to provide information on the dissolved oxygen environment in the plant root zone for the optimum control of hydroponics and solid substrate plant cultivation systems in the space environment. Miniaturized polarographic dissolved oxygen sensors have been designed and fabricated on a flexible Kapton® (polyimide) substrate. Two capabilities of the new microsensor array were explored. First, measurements of dissolved oxygen in the plant root zone in hydroponics and solid substrate culture systems were made. The microsensor array was fabricated on a flexible substrate, and then cut out into a mesh type to make a suspended array that could be placed either in a hydroponics system or in a solid substrate cultivation system to measure the oxygen environments. Second, the in situ self-diagnostic and self-calibration capability (two-point for oxygen) was adopted by dynamically controlling the microenvironment in close proximity to the microsensors. With a built-in generating electrode that surrounds the microsensor, two kinds of microenvironments (oxygen-saturated and oxygen-depleted phases) could be established by water electrolysis depending on the polarity of the generating electrode. The unique features of the new microsensor array (small size, multiple sensors, flexibility and self-diagnosis) can have exceptional benefits for the study and optimization of plant cultivation systems in both terrestrial and microgravity environments. The in situ self-diagnostic and self-calibration features of the microsensor array will also enable continuous verification of the operability during entire plant growth cycles. This concept of automated control of a novel chemical monitoring system will minimize crew time required for maintenance, as well as reduce volume, mass, and power consumption by eliminating bulky diagnosis systems including calibrant (fluid and gas) reservoir and flow system hardware. [This research was funded partly by a grant from the NASA Office of Biological and Physical Research (01-OBPR-01)]
Key words: Oxygen; Root; Kapton; Calibration

*Abstract MC26*

**Electrochemical Sensor Arrays for Analysis of Water Quality in Space Habitats**

Prof. Samuel Kounaves
*Professor, Department of Chemistry, Tufts University*

Brian Comeau
*Graduate Research Assistant, Department of Chemistry, Tufts University*

Stefan Lukow
*Graduate Research Assistant, Department of Chemistry, Tufts University*

Martin Buehler
*Senior Scientist, MS 302-231, Jet Propulsion Laboratory*

*Correspondence:* Prof. Samuel Kounaves, Professor, Department of Chemistry, Tufts University, 62 Talbot Avenue, Medford, MA 02155, USA. Phone: 617-627-3124; Fax: 617-627-3443; E-mail:

One of the main components of NASA's Advanced Human Support Technologies for Environmental Monitoring & Control is the research and development of systems for monitoring the chemical and physical status of life support systems and their resources. One critical component of this system is the water supply and is accompanying chemical and biological purification subsystem. All water which can come into contact with humans, internally or externally, must be continuously or regularly monitored. The in situ or online monitoring systems must provide a reliable real time measure of water quality by identification and quantification of a broad spectrum of chemical components, including relevant anionic and cationic species, and other water quality parameters. The goal of this research project has been aimed at developing a rugged, reliable, low-power electrochemically based sensor array representing a new integrated approach to quantitative analytical and chemometric chemical monitoring. The resulting sensor consists of an array of specific and semispecific ion selective and amperometric transducers, which can simultaneously and continuously identify and semiquantitatively determine over 30 inorganic analytes in both drinking water and waste water (in effect an electronic tongue). The fabrication, integration, and multiplexing of such a large number of ion selective electrodes (ISEs) on a single substrate, for use in analysis of such a complex mixture of chemical species, has not been previously attempted. We present here the results of our effort and discuss the challenges in terms of scaling of the electrochemical ion selective ionophore-based transduction mechanisms, the selection and immobilization of appropriate ionophore matrices and substrates, lifetime, sampling & data treatment issues, and other critical issues of flow-through chemical analysis in microgravity environments. The device will eventually be demonstrated for flight-based water quality and chemical monitoring on an appropriate platform such as the International Space Station, NG Launch Vehicles, Lunar, and Martian Habitats.
Key words: Water quality; Sensor arrays; Ion selective; Chemical analysis

*Abstract MC27*

**An Expert System for Optimization of Watering for a Mars Greenhouse**

Slide 1

# Flexible Microsensor Array for the Monitoring and Control of Plant Growth System

Chang-Soo Kim[1,2], D. Marshall Porterfield[2,1], H. Troy Nagle[3,4], Christopher S. Brown[5]

(1) Electrical & Computer Eng., Univ. of Missouri-Rolla
(2) Biological Sciences, Univ. of Missouri-Rolla
(3) Electrical & Computer Eng., North Carolina State Univ.
(4) Joint Dept. of Biomedical Eng., Univ. of North Carolina-Chapel Hill / North Carolina State Univ.
(5) Kenan Institute for Eng., Tech., & Science, North Carolina State Univ.



Slide 2

## Plant growth platform in microgravity

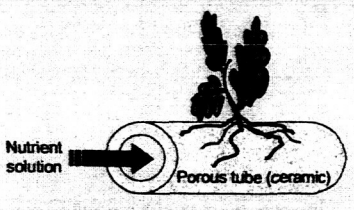


- Nutrient solution delivery using porous layer; capillary interface between root and solution.
- Critical need of precise control of rhizosphere (root-environment interactions); wetness, oxygen, nutrients, temperature, etc.



Slide 3

## Requirements for sensors in monitoring and control of root zone

- Ideal configuration; miniaturization, multiple, low power consumption, robustness and stability.
- Dependable "*In situ* diagnosis and/or calibration" method; maintenance of accuracy and functionality.
- Microsensors for dissolved oxygen and wetness detection.

Slide 4

## Electrochemical microelectrodes on polyimide (Kapton®) substrate (3-electrode polarographic oxygen sensor)

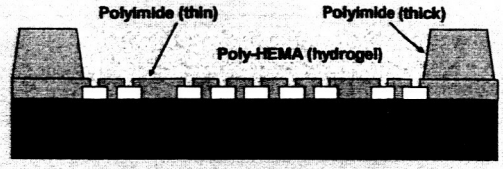


- Substrate: Kapton (polyimide)
- Metal (Pt) and lithography
- Polyimide lithography (thin)
- Polyimide lithography (thick)



Slide 5

## Microsensor arrays on flexible substrates

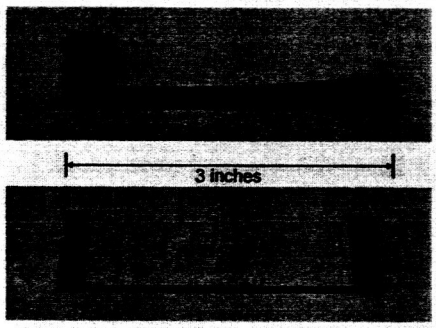


- Oxygen microsensor strip (3-electrode electrochemical measurement)
- Conductivity sensor strip (4-electrode impedance measurement)



Slide 6

## Porous tube - microsensor interface (animation)

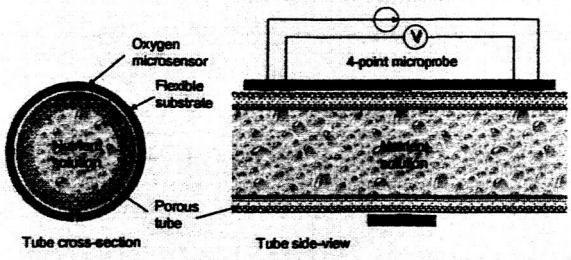


- Microsensor array on a flexible substrate enwrapping a porous tube.
- Oxygen microsensor; dissolved oxygen detection.
- 4-point microprobe: surface wetness detection.

Slide 7

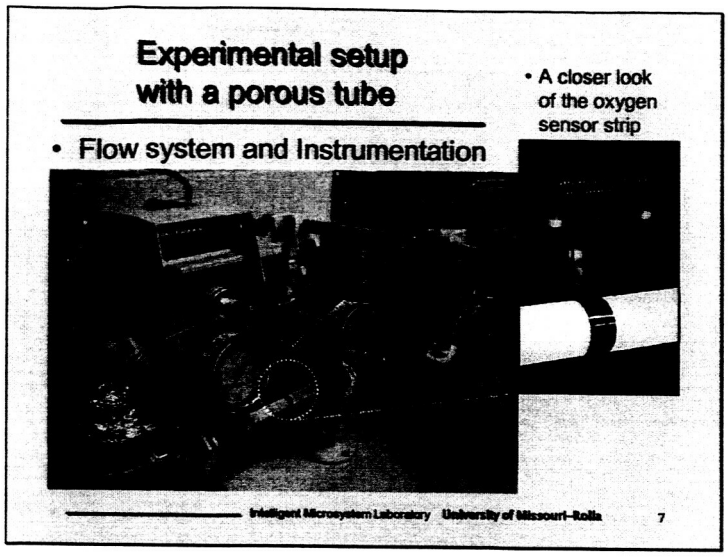


Slide 8

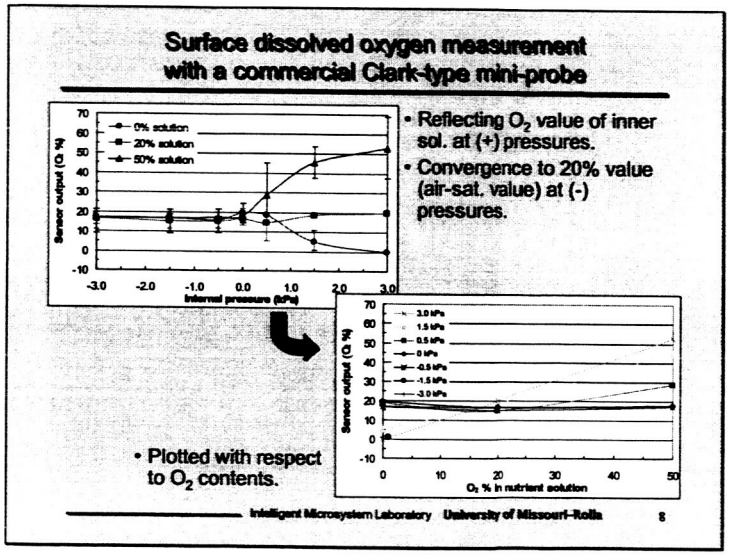


Slide 9

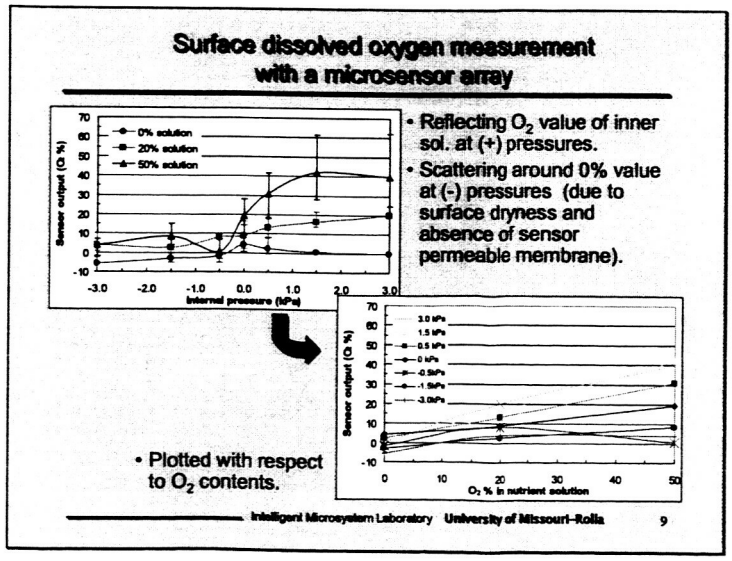

Slide 10

## Surface wetness measurement with a 4-point microprobe array

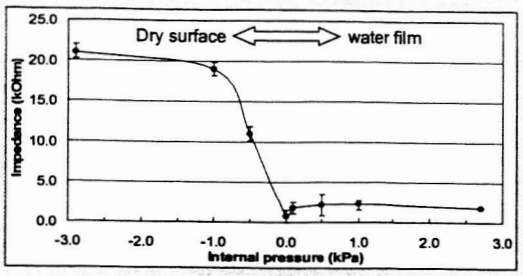


- A steep decrease of surface impedance at the transition from (-) to (+) pressure.



Slide 11

## On-chip intelligence of dissolved oxygen microsensor with built-in microactuator; *in situ* self-diagnosis

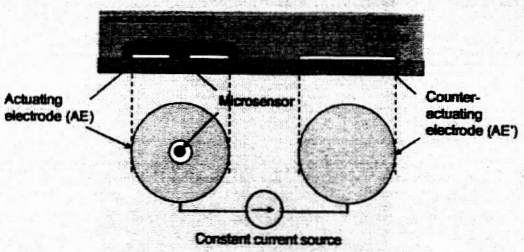


- $O_2$-rich or $O_2$-depleted microenvironments established by water electrolysis.
- $2H_2O \rightarrow 4H^+ + 4e^- + O_2$ (at AE as anode)
- $2H_2O + 2e^- \rightarrow 2OH^- + H_2$ (at AE as cathode)



Slide 12

## Sensor responses during $O_2$-generating actuation phases with various current densities (in bulk solution)

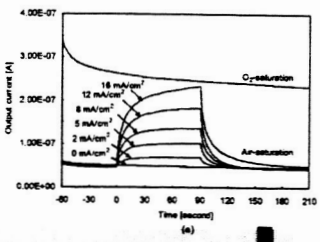


- Approaching to $O_2$-saturation value with increasing actuation current density.

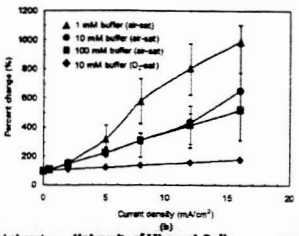


- Response ratio (saturation @t=90 / baseline @t=0).
- "Excessive" responses (beyond 476%, i.e. 100%/21%).

Slide 13

## Why excessive response (over 476%)?

1. Super-saturation;
   excessive solubility of electrochemically generated dissolved gas near the electrode.
2. pH shift accompanying to the gas generation;
   dependence of the oxygen reduction coefficient (catalytic activity) on solution pH.

- In low pH (n=4); $O_2 + 2H_2O + 4e^- \rightarrow 4OH^-$
- In high pH (n=2); $O_2 + 2H_2O + 2e^- \rightarrow H_2O_2 + 2OH^-$, $H_2O_2 + 2e^- \rightarrow 2OH^-$



Slide 14

## Why excessive response ? (continued)

3. Pseudo-convection;
   concentration-driven convection from the AE to enhance the mass transfer of oxygen to the WE.
4. Electrochemical interference;
   "feedback" of $H_2O_2$ to be converted at AE ($H_2O_2 \rightarrow 2H^+ + O_2 + 2e^-$, byproduct of oxygen reduction @WE).
5. Temperature;
   local temperature elevation due to high current density in AE.



Slide 15

## Sensor responses during $O_2$-depleting actuation phases with various current densities (in bulk solution)

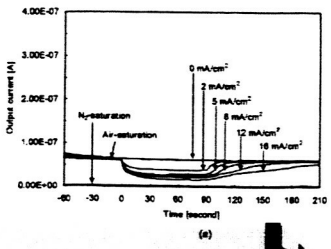


- Approaching $N_2$-saturation ($O_2$-depletion) value with increasing actuation current density.

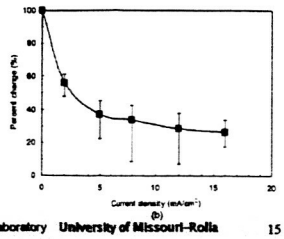


- Response ratio (saturation @t=90 / baseline @t=0).

Slide 16

## Summary

- Demonstration of feasibility of microsensor for porous tube surface measurements.
  - Dissolved oxygen.
  - Wetness.
- Demonstration of built-in, on-chip intelligence (*in situ* self- diagnosis/calibration).
  - Controlled oxygen microenvironments with an integrated actuator.
  - Need of an external permeable membrane.
  - Functional integration as well as structural integration.



Slide 17

## Summary (continued)

- Current work in progress
  - microsensor for plant growth platform + *in situ* intelligence
- Prospects for microscale water electrolysis
  - Microsensor application; oxygen, pH.
  - Microactuator application; microfluidics for pumping/dosing, microreactor, *in situ* $O_2$ generation near root zone.

Acknowledgement:
NASA grant 01-OBPR-01.